

Rongyao Cai ^{*1} Yuxi Wan ^{*1} Kexin Zhang ¹ Ming Jin ² Hao Wang ³
 Zhiqiang Ge ⁴ Daoyi Dong ⁵ Yong Liu ¹ Qingsong Wen ⁶

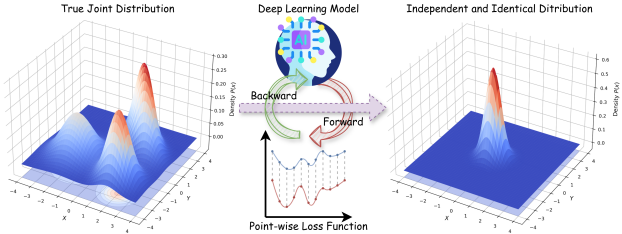


Figure 1: Motivation of our work. The use of a point-wise loss function leads to the deep learning model to presume an independent and identical distribution as an approximation for the true joint distribution of data. It is biased.

Abstract

Optimizing time series models via point-wise loss functions (e.g., MSE) relying on a flawed *point-wise independent and identically distributed (i.i.d.) assumption* that disregards the causal temporal structure, an issue with growing awareness yet lacking formal theoretical grounding. Focusing on the core independence issue under covariance stationarity, this paper aims to provide a **first-principles analysis of the Expectation of Optimization Bias (EOB)**, formalizing it information-theoretically as the discrepancy between the true joint distribution and its flawed i.i.d. counterpart. Our analysis reveals a **fundamental paradigm paradox**: the more deterministic and structured the time series, the more severe the bias by point-wise loss function. We derive the *first closed-form quantification* for the **non-deterministic EOB** across linear and non-linear systems, and prove EOB is an intrinsic data property, governed exclusively by *sequence length* and our proposed *Structural Signal-to-Noise Ratio (SSNR)*. This theoretical diagnosis motivates our **principled debi-**

asing program that eliminates the bias through *sequence length reduction* and *structural orthogonalization*. We present a concrete solution that simultaneously achieves both principles via DFT or DWT. Furthermore, a novel **harmonized ℓ_p norm framework** is proposed to rectify gradient pathologies of high-variance series. Extensive experiments validate EOB Theory’s generality and the superior performance of debiasing program.

1. Introduction

Time series analysis is a foundational task in machine learning (Zhang et al., 2024), with applications spanning economics (Zhang et al., 2025; Bao et al., 2025), industry (Cai et al., 2024), and healthcare (Li et al., 2024). The performance of deep learning models in this domain primarily depends on two core perspectives: the expressive power of the network architecture and the rationality of the training paradigm, particularly the loss function design.

Model expressiveness has been the primary focus of the research community. This has led to a vibrant and rapidly evolving landscape of complex architectures, from foundational RNNs (Kong et al., 2025), CNNs (Donghao & Xue, 2024) and GNNs (Chen et al., 2024b) to the current struggle for supremacy among the Transformer family (Liu et al., 2024; Chen et al., 2024a; Jin et al., 2024b), advanced MLPs (Ekambaram et al., 2023) and Diffusion (Rasul et al., 2021) in temporal domain. Concurrently, modeling in the frequency domain has emerged as a powerful new force (Yi et al., 2023b; 2025; Yang et al., 2024; Zhong et al., 2025; Cheng et al., 2025; Xu et al., 2024; Crabbé et al., 2024), with lightweight linear models demonstrating surprisingly superior performance over heavyweight architectures.

In stark contrast, the rationality of training paradigm that arguably determines the upper limit of model performance, has remained largely unexamined. The optimization of models via point-wise loss functions (e.g., MSE, MAE) in temporal domain is the standard paradigm for almost forecasting, imputation, and anomaly detection tasks (Jin et al., 2024a). While intuitive, *this approach is built on a heuristic point-wise independent and identically distributed*

^{*}Equal contribution ¹Institute of Cyber-Systems and Control, Zhejiang University ²Griffith University ³Xiaohongshu Inc. ⁴School of Mathematics, Southeast University ⁵University of Technology Sydney ⁶Squirrel Ai Learning. Correspondence to: Kexin Zhang <zhangkexin@zju.edu.cn>, Ming Jin <ming.jin@griffith.edu.au>.

(*i.i.d.*) *assumption*, which fundamentally conflicts with the causal, temporal structure that defines time series data with dynamic characteristics, as illustrated in Figure 1. This “*i.i.d.*” assumption contains two distinct flaws: the *identically distributed* assumption, which is violated by dynamic non-stationarity, and the *independence* assumption, which is violated by temporal causality. We argue that the **independence issue** is the more foundational one, as it has a fundamental conflict with the contextual causality inherent in time series. We therefore focus on isolating this core independence issue, which allows us to build a rigorous theory under the well-defined conditions of *covariance-stationarity*.

Recent studies have begun to confront this issue. Works such as FreDF (Wang et al., 2025b) and Time-01 (Wang et al., 2025a) explore this issue from the perspective of “label autocorrelation”, yet their analysis remains preliminary; the bias is defined as a posteriori effect dependent on a known model output, failing to identify the core, a prior factors that govern it. Another line of research engineers more sophisticated loss functions. For instance, PSLoss (Kudrat et al., 2025) incorporates local similarity measures akin to PatchTST (Nie et al., 2023), while DBLoss (Qiu et al., 2025) explicitly decomposes trend and periodic components to balance their optimization contributions. Despite their empirical success, like the faint light before dawn, the motivation for these methods remains largely heuristic, lacking a systematic theoretical framework to explain the underlying optimization pathology.

To cut through this fog of heuristic exploration, this paper ambitiously establishes the **first-principled, systematic theoretical analysis** of the optimization bias stemming from the *point-wise independence assumption*. Wielding the tools of information theory and stochastic process modeling (Ross, 2023), we chart a clear path from diagnosis to prescription. We begin by defining the **Expectation of Optimization Bias (EOB)** as the probabilistic divergence, *i.e.*, KL-divergence, between the true joint distribution and the flawed factorized distribution assumed by point-wise loss function. This formalization allows us to uncover the bounds of EOB and reveal a fundamental **Paradigm Paradox: the more deterministic the process, the more severely it is penalized by point-wise loss, a finding that depends purely on the data’s intrinsic properties**.

Our analysis proves that the lower bound of the EOB is governed by the non-deterministic component of the process. We therefore proceed to quantify this lower bound for both linear (parametric *autoregressive model* and non-parametric *multivariate Gaussian model*) and non-linear (*Gaussian mixture model*) systems, abstracting its decisive factors (*i.e.*, *sequence length* and *structural signal-to-noise ratio*). Based on this solid theoretical diagnosis, we propose a **Principled Debiasing Program** that not only provides a

unifying framework for existing methods but also motivates a novel and robust solution. Concretely, we instantiate our program through Discrete Fourier Transform (DFT). Moreover, we improve the optimization robustness in frequency domain via a novel **harmonized ℓ_p norm framework** to resolve the gradient pathologies.

To summarize, our contributions include:

- **Formalization of Paradigm Paradox:** This work is the first to formalize systematic analysis of the optimization bias inherent to point-wise loss functions, which stems from their heuristic *i.i.d.* assumption. We derive bounds on EOB, revealing a fundamental paradigm paradox: the more deterministic a time series, the more severely it is penalized by the point-wise loss.
- **Quantification of EOB Lower Bound:** We present the first closed-form quantification of non-deterministic EOB for linear process, unifying the analysis of parametric and non-parametric models. We further extend this theory to non-linear processes.
- **Fundamental Nature of the Bias:** We prove that the lower bound is a basic data property governed solely by sequence length and defined Structural Signal-to-Noise Ratio (SSNR) of stochastic component, regardless of point-wise loss formula or model architecture utilized.
- **Principled Debiasing Program:** We propose an essential principle that eliminates the bias. Furthermore, a concrete solution is introduced using DFT or DWT with a harmonized ℓ_p norm optimization to resolve gradient pathologies of high-variance series.
- **Comprehensive Empirical Validation:** Experiments on synthetic and real-world benchmarks validate the generality of our EOB Theory and debiasing program.

2. Optimization Bias of Point-wise Loss

Our theory first establishes a formal definition and the lower bound for EOB in Section 2.1. We then quantify the non-deterministic EOB in linear systems through both dynamic and correlational insights, using a parametric autoregressive model (Section 2.1.1) and a non-parametric multivariate Gaussian model (Section 2.2.2), and derive a unified expression. Finally, we extend these linear findings to non-linear conditions via Gaussian mixture model in Section 2.3.

2.1. Formalization of Probability Distribution Divergenc

In machine learning, the minimization of a training loss is implicitly equivalent to maximizing the likelihood of a probabilistic model, $q(x_{1:T})$, which serves as an approximation

of the true data-generating distribution, $p(x_{1:T})$. The ubiquitous use of point-wise loss functions (e.g, MSE, MAE) introduces a critical flaw by incorrectly assuming that each data point in a sequence is conditionally independent. We term this the **point-wise independence assumption**:

$$q(x_{1:T}) = \prod_{t=1}^T p(x_t). \quad (1)$$

However, the defining characteristic of a time series is its temporal structure, where observations are sequentially dependent. The true joint probability distribution, $p(x_{1:T})$, must therefore be expressed using the chain rule of probability to respect this inherent auto-correlation:

$$p(x_{1:T}) = p(x_1) \cdot \prod_{t=2}^T p(x_t|x_{1:t-1}). \quad (2)$$

This reveals a fundamental discrepancy between the training objective and the true data structure. By decomposing the true log-likelihood, $\log p(x_{1:T})$, we can precisely quantify the divergence introduced by the point-wise independence assumption:

$$\log p(x_{1:T}) = \underbrace{\sum_{t=1}^T \log p(x_t)}_{\text{Implicit Objective}} + \underbrace{\sum_{t=2}^T \log \frac{p(x_t|x_{1:t-1})}{p(x_t)}}_{\text{Correction Term}}. \quad (3)$$

We define this correction term as the **Optimization Bias \mathcal{B}** of point-wise loss. It represents the accumulated information gain from conditioning on the past, a factor completely overlooked when a model is trained by minimizing a simple sum of independent errors.

To analyze the properties of this bias, we can bound its expectation by considering the composition of the time series.

Theorem 2.1. (Bounds on the Expectation of Optimization Bias) Let $\{x_t\}$ be a process admitting a Cramér decomposition $x_t = v_t + z_t$, where $\{v_t\}$ is the deterministic component and $\{z_t\}$ is the purely stochastic component. Assume the following conditions hold:

1. **Determination:** v_t is perfectly predictable from its past $v_{1:t-1}$, such that conditional entropy $H(v_t|v_{1:t-1}) = -\infty$.
2. **Independence:** $\{v_t\}$ and $\{z_t\}$ are independent.
3. **Information Equivalence:** The information contained in the history $x_{1:t-1}$ is equivalent to that in $\{v_{1:t-1}, z_{1:t-1}\}$.

Then, the expectation of optimization bias of the sequence x_t over a duration T , $\mathbb{E}[\mathcal{B}]$, is bounded as follows:

$$\mathbb{E} \left[\sum_{t=2}^T \log \frac{p(z_t|z_{1:t-1})}{p(z_t)} \right] \leq \mathbb{E}[\mathcal{B}] \leq \mathbb{E} \left[\sum_{t=2}^T \log \frac{p(v_t|v_{1:t-1})}{p(v_t)} \right] \quad (4)$$

Proof. See Appendix A.

The upper bound in Theorem 2.1 (Cramér, 1946), driven by the deterministic component's bias, approaches infinity for any non-trivial deterministic process. This leads to a counterintuitive conclusion, formalized as a paradox.

Theorem 2.2. (Paradigm Paradox of Point-wise Loss)

The more deterministic a process, the greater the optimization bias incurred by a point-wise loss function.

As the upper bound of $\mathbb{E}[\mathcal{B}]$ is infinite for any non-trivial deterministic process, a meaningful analysis requires focusing on its lower bound, *i.e.*, the expectation of optimization bias of the non-deterministic component, $\{z_t\}$. We formally term this quantity the **non-deterministic Expectation of Optimization Bias (EOB)** and aim to quantify it:

$$\mathbb{E}[\mathcal{B}_z] = \mathbb{E} \left[\sum_{t=2}^T \log \frac{p(z_t|z_{1:t-1})}{p(z_t)} \right]. \quad (5)$$

2.2. Linear Modeling of Non-deterministic EOB

2.2.1. PARAMETRIC AUTOREGRESSIVE MODEL

To make the non-deterministic EOB concrete, we begin by deriving a closed-form expression using a canonical stochastic process: the covariance-stationary autoregressive model of order p , defined as $AR(p)$:

$$z_t = c + \sum_{i=1}^p \phi_i z_{t-i} + \epsilon_t \quad (6)$$

where $\{\phi_i\}$ denotes the autoregressive coefficients, c is a constant, and $\{\epsilon_t\}$ is a white noise process of innovations with $\mathbb{E}[\epsilon_t] = 0$, $\text{Var}[\epsilon_t] = \sigma_\epsilon^2$, and $\text{Cov}(\epsilon_i, \epsilon_j) = 0$ if $i \neq j$.

Proposition 2.3. (Quantification of Non-deterministic EOB via $AR(p)$) For any covariance-stationary Gaussian process driven by $AR(p)$, the non-deterministic EOB, $\mathbb{E}[\mathcal{B}_z]$, incurred by a point-wise loss function is quantified by:

$$\mathbb{E}[\mathcal{B}_z] = \frac{T-p}{2} \log \frac{\sigma_z^2}{\sigma_\epsilon^2} = \frac{T-p}{2} \log \frac{1}{1 - \sum_{i=1}^p \phi_i \rho_i} \quad (7)$$

where ϕ_i and ρ_i are the autoregressive coefficient and autocorrelation function at lag i , respectively.

Proof. See Appendix B.

This result is profound and can be deconstructed into two key factors: *Sequence Length* ($T-p$), over which the EOB accumulates linearly, and *variance ratio* ($\sigma_z^2/\sigma_\epsilon^2$). The latter term is a significant statistics, formalized as follows:

Definition 2.4. (Structural Signal-to-Noise Ratio) For any covariance-stationary process, SSNR is the ratio of the total unconditional variance (σ_z^2) to its one-step-ahead optimal prediction error variance (σ_ϵ^2):

$$SSNR = \frac{\sigma_z^2}{\sigma_\epsilon^2} = \frac{\text{Var}(z_t)}{\text{Var}(z_t - \mathbb{E}[z_t|z_{1:t-1}])} \quad (8)$$

where $\mathbb{E}[z_t|z_{1:t-1}]$ is the optimal prediction of z_t given all past information, and the denominator represents the variance of the process's irreducible innovation.

Conceptually, SSNR measures the ratio of a process's *total uncertainty* to its *residual uncertainty*. A high SSNR signifies a process with strong internal structure and high predictability. A key property of SSNR within the $AR(p)$ model is its exclusive dependence on the intrinsic autoregressive coefficients ϕ_i , rendering it a pure measure of the series's internal structure, independent of the noise scale. The relationship between our defined SSNR and classical SNR is further detailed in Appendix C.

2.2.2. NON-PARAMETRIC MULTIVARIATE GAUSSIAN MODEL

While the preceding analysis provides a closed-form solution for a parametric $AR(p)$ process, we now generalize this result to a broader, non-parametric condition. Considering any linear, covariance-stationary process can be driven by a **Multivariate Gaussian Model (MGM)**, it leads to an elegant and fundamental principle governing $\mathbb{E}[\mathcal{B}_z]$.

$$z \sim \mathcal{N}(\mu, \Sigma). \quad (9)$$

Proposition 2.5. (Quantification of Non-deterministic EOB via MGM) For any stochastic, covariance-stationary process modeled by a multivariate Gaussian distribution, the non-deterministic EOB, is determined solely by the determinant of correlation matrix, $|R|$:

$$\mathbb{E}[\mathcal{B}_z] = -\frac{1}{2} \log |R|. \quad (10)$$

Proof. See Appendix D.1.

At first glance, the non-parametric expression in (10) appears distinct from its parametric $AR(p)$ counterpart in (7). However, we will prove they are fundamentally consistent.

For an *infinite forecast horizon* ($T \rightarrow \infty$), we establish their asymptotic equivalence. As proven in Lemma D.1 (Appendix D.2), the determinant $|R|$ has the following limit:

$$\lim_{T \rightarrow \infty} |R|^{1/T} = \frac{\sigma_\epsilon^2}{\sigma_z^2} = \frac{1}{SSNR}. \quad (11)$$

This identity reveals that the asymptotic forms derived from

MGM and $AR(p)$ are identical when considering average EOB per timestep:

$$\lim_{T \rightarrow \infty} -\frac{1}{2T} \log |R| = \lim_{T \rightarrow \infty} \frac{1}{2} \log \frac{1}{|R|^{1/T}} = \frac{1}{2} \log(SSNR). \quad (12)$$

For a *finite horizon* T , we can bridge the gap exactly. As proven in Lemma D.2 (Appendix D.2), $|R|$ for a covariance-stationary $AR(p)$ process can be decomposed precisely as:

$$|R| = |R_p| \cdot \left(\frac{\sigma_\epsilon^2}{\sigma_z^2} \right)^{T-p} \quad (13)$$

where $|R_p|$ is the determinant of the correlation matrix of the initial p observations.

Substituting this identity into the MGM formula (10) yields:

$$\mathbb{E}[\mathcal{B}_z] = -\frac{1}{2} \log |R| = \frac{T-p}{2} \log \frac{\sigma_z^2}{\sigma_\epsilon^2} - \frac{1}{2} \log |R_p|. \quad (14)$$

This result provides a profound insight, unifying the parametric and non-parametric perspectives. It reveals that the total non-deterministic EOB is composed of two parts: a primary term, $\frac{T-p}{2} \log(SSNR)$, which represents the bias accumulated during the $T-p$ steady-state steps, and a constant correction term, $-\frac{1}{2} \log |R_p|$, accounting for the bias from the initial p -step transient phase. This unification culminates in a central theorem for quantifying the EOB.

Theorem 2.6. (Quantification of Non-deterministic EOB) For any covariance-stationary process, the non-deterministic EOB, $\mathbb{E}[\mathcal{B}_z]$, incurred by a point-wise loss is fundamentally determined by the sequence length T and its SSNR, and can be expressed as:

$$\mathbb{E}[\mathcal{B}_z] = \frac{T}{2} \log(SSNR) + c \quad (15)$$

where $c = -\frac{1}{2} \log(|R_p| \cdot (SSNR)^p)$ is a constant only relying on the initial short-term memory of the process.

2.3. Non-linear Modeling of Non-deterministic EOB

To extend our analysis beyond linear systems, we now consider nonlinear, nondeterministic systems. A canonical approach for modeling such complexity is the **Gaussian Mixture Model (GMM)**, representing the process distribution as a weighted sum of multiple Gaussian components:

$$p(z) = \sum_{k=1}^K \pi_k \mathcal{N}(z_k | \mu_k, \Sigma_k) = \sum_{k=1}^K \pi_k p(z_k) \quad (16)$$

where $p(z_k)$ represents the k -th Gaussian component and π_k is its corresponding mixture weight.

Directly computing the non-deterministic EOB for a GMM is analytically intractable due to the logarithm-of-sums form, $\log \left(\sum_{k=1}^K \pi_k p(z_k) \right)$, inherent in its log-likelihood. To overcome this obstacle, we reformulate the EOB using the language of information theory. By the *Jensen’s Inequality*, we have the lower bound of GMM non-deterministic EOB, detailed in Appendix E:

$$\mathbb{E}[\mathcal{B}_z] \geq \sum_{k=1}^K \pi_k \mathbb{E}[\mathcal{B}_k] - H(\pi). \quad (17)$$

This derivation yields a powerful insight: the lower bound of non-deterministic EOB for a GMM is the weighted average of the EOBs of its individual Gaussian components, $\mathbb{E}[\mathcal{B}_k]$, penalized by the Shannon entropy of the mixture weights, $H(\pi)$. Specifically, $\mathbb{E}[\mathcal{B}_k]$ can be quantified using our previous findings (e.g., Eq. (15)).

3. Discussion and Limitation of EOB Theory

3.1. Information-Theoretic Interpretation and Thinking

From an information-theoretic perspective, the non-deterministic EOB, $\mathbb{E}[\mathcal{B}_z]$, quantified in Theorem 2.6 and Eq. (17) is precisely the Kullback-Leibler (KL) divergence between the true joint distribution $P(z_{1:T})$ and the factorized distribution $Q(z_{1:T}) = \prod_{t=1}^T p(z_t)$ implicitly shielded by the point-wise independence assumption.

$$D_{KL}(P\|Q) = \mathbb{E}_{z \sim P} \left[\log \frac{p(z_{1:T})}{q(z_{1:T})} \right] = \mathbb{E}[\mathcal{B}_z]. \quad (18)$$

This perspective, combined with our quantitative results, culminates in a central insight, which we formalize as the **Non-deterministic Penalty** of the point-wise training paradigm.

Theorem 3.1. (Non-deterministic Penalty of Point-wise Loss) *The longer a covariance-stationary process and the higher its SSNR, the greater the non-deterministic EOB, $\mathbb{E}[\mathcal{B}_z]$, incurred by point-wise independence assumption, i.e., a greater lower bound of $\mathbb{E}[\mathcal{B}]$.*

This seemingly counter-intuitive result is the core of our analysis and aligns with the Paradigm Paradox (Theorem 2.2). $\mathbb{E}[\mathcal{B}_z]$ represents the irreducible lower bound of the total EOB, $\mathbb{E}[\mathcal{B}]$, stemming from the flawed *point-wise independence assumption*. This flaw is inherent to any point-wise loss function itself, irrespective of the model architecture being trained. Consequently, the more pronounced the internal structure of a sequence, the more critical temporal information is discarded. This leads to a powerful conclusion: data with the strongest structural signal is penalized most heavily by a structure-agnostic loss function.

This paradox offers a new theoretical lens to correct a classic empirical misdiagnosis: *the difficulty of training simple mod-*

els like MLPs on highly periodic data (Ziyin et al., 2020), stems not from limited model expressiveness, as often assumed, but from a fundamental optimization pathology. Our analysis confirms the problem is more fundamental, stemming not from the model, but from an optimization pathology. The inherent point-wise independence assumption actively works against learning the temporal structure of the data, fundamentally misaligned with the learning objective.

Critically, our findings reveal this optimization bias is fundamentally immune to the community’s current solutions: the bias cannot be eliminated by simply enhancing model capacity (e.g., using stronger networks (Wang et al., 2025c) or LLM (Jin et al., 2024b;c)) or employing more sophisticated optimization algorithms. As long as the training objective relies on the point-wise independence assumption, this inherent flaw will persist.

3.2. Moreover

More interesting discussions of the limitations and further work on EOB Theory are provided in Appendix F.

4. A Principled Debiasing Program

Having diagnosed the theoretical origins of EOB (Section 2), we now transition from diagnosis to prescription by proposing a principled framework designed to eliminate the bias.

Strategy 1: Statistical Alignment. Rather than modifying the temporal MSE loss function $\mathcal{L}_{\text{TMSE}}$ directly, a common heuristic approach to mitigate optimization bias is to introduce auxiliary terms that align local or global statistics \mathcal{S} . However, these adjusted loss functions do not address the root cause of EOB. Instead, they merely alleviate the independence issue of temporal MSE by imposing stronger external statistical constraints,

$$\hat{\mathcal{L}} = \mathcal{L}_{\text{TMSE}} + \mathcal{L}(\mathcal{S}). \quad (19)$$

Our theoretical analysis has unequivocally shown that optimization bias is driven by two fundamental factors: the sequence length (T) and the SSNR. This diagnosis directly motivates a two-pronged “*Debiasing Program*” to tackle these two drivers by reshaping the optimization landscape.

Strategy 2: Sequence Length Reduction. Since EOB grows with sequence length, the intuitive strategy is to reduce the length of optimization target. This can be achieved by applying a reversible *compression operator*, $\mathcal{T}_{\text{comp}}(\cdot)$, which maps the target sequence to a more compact representation of length $T' < T$. The model is then trained to predict this compressed target. After optimization, the full-length forecast is recovered via the inverse operator, $\mathcal{T}_{\text{comp}}^{-1}(\cdot)$,

$$\hat{x}_c = \mathcal{T}_{\text{comp}}(x) \in \mathbb{R}^{T'}, x = \mathcal{T}_{\text{comp}}^{-1}(\hat{x}_c) \in \mathbb{R}^T, T' < T. \quad (20)$$

Strategy 3: Structural Orthogonalization. While above strategies mitigates the bias, a more fundamental solution targets its root cause: the temporal correlation encapsulated by the SSNR. By transforming the optimization target into a basis of mutually orthogonal components, we can make the point-wise independence assumption valid in the transformed domain. We propose using a reversible *orthogonality operator*, $\mathcal{T}_{\text{ortho}}(\cdot)$, to decompose the correlated series into uncorrelated components. Optimizing in this new domain effectively sets the SSNR to its theoretical minimum of one, eliminating the source of optimization bias entirely,

$$\begin{aligned} \hat{x}_o &= \mathcal{T}_{\text{ortho}}(x), \quad x = \mathcal{T}_{\text{ortho}}^{-1}(\hat{x}_o) \\ \text{s.t. } \text{Cov}(\hat{x}_o) &= \text{diag}(\sigma_1^2, \dots, \sigma_T^2). \end{aligned} \quad (21)$$

5. A Concrete Solution via Fourier Transform

To instantiate the principles of the *Debiasing Program*, we select the *Discrete Fourier Transform* (DFT) as a canonical and highly effective implementation. The DFT is uniquely suited to this task as its key advantages: 1) approximate orthogonality decomposition and 2) exceptional computational efficiency with complexity $\mathcal{O}(L \log L)$. The comprehensive analysis of these advantages is provided in Appendix G.1. Furthermore, we demonstrate a rigorous gradient analysis of various DFT applications in Appendix H, yielding a genuinely effective optimization path.

Notably, global basis functions of DFT are ill-suited for decomposing non-stationary systems, while dynamic characteristics are widespread in practice to reduce SSNR. *Discrete Wavelet Transform* (DWT) emerges as a more practical alternative, leveraging its time-frequency localization capabilities and demonstrating superior performance in characterizing dynamic and localized patterns (See Appendix G.2).

5.1. Gradient Pathology Analysis of ℓ_p Norm

While the structural orthogonalization like DFT or DWT provides a theoretically sound solution, it introduces a new, practical challenge during training: the high dynamic range of the orthogonal elements, a scenario where standard ℓ_p norms exhibit critical optimization pathologies.

The ℓ_2 norm suffers from *gradient dominance*: its gradient is proportional to the absolute error, causing high-magnitude components to overwhelm the learning process and leave weaker components under-optimized. Conversely, the ℓ_1 norm's constant-magnitude gradient leads to *gradient fatigue*: the uniform dynamic is too weak to drive large-magnitude components to convergence effectively, while may be too aggressive for small-magnitude components, causing overshooting. A detailed mathematical analysis of these gradient pathologies is provided in Appendix G.3.

5.2. Harmonized ℓ_p Norm Optimization

To resolve these duality of flaws, we propose the *Harmonized ℓ_p Norm* ($\mathcal{L}_{\text{Harm}, \ell_p}$), a framework that dynamically re-weights the gradient for each component based on its historical magnitude, \bar{f}_k .

5.2.1. TO MITIGATE DOMINANCE FOR ℓ_2

Harmonized MSE (hMSE) up-weights the gradient of *weaker components* by incorporating a relative error term:

$$\mathcal{L}_{\text{Harm}, \ell_2} = \sum_{k=1}^K \left(1 + \frac{\gamma}{\bar{f}_k + \epsilon} \right) \|f_k - \hat{f}_k\|_2^2 \quad (22)$$

where γ is a factor balancing the two terms, and ϵ denotes the minimum threshold preventing explosion.

5.2.2. TO CURE FATIGUE FOR ℓ_1

Harmonized MAE (hMAE) amplifies the gradient for *stronger components* by scaling the loss to be proportional to each component's magnitude:

$$\mathcal{L}_{\text{Harm}, \ell_1} = \sum_{k=1}^K (1 + \gamma \bar{f}_k) \|f_k - \hat{f}_k\|_1. \quad (23)$$

In practice, the component magnitude \bar{f}_k is estimated efficiently and robustly via an Exponential Moving Average (EMA) updated at each training iteration e :

$$\bar{f}_k^{(e+1)} = \beta \bar{f}_k^{(e)} + (1 - \beta) |f_k^{(e)}| \quad (24)$$

where β is the smoothing factor.

This adaptive re-weighting mechanism provides a stable scaling factor for both hMSE and hMAE, and since it only requires storing and updating the EMA, the entire harmonization process adds negligible $\mathcal{O}(K)$ computational overhead, making it a highly practical solution.

5.2.3. STATISTICAL ANALYSIS OF HARMONIZED NORM

We prove that the harmonized ℓ_p norm achieves both point-estimation and information-theoretic unbiasedness. Furthermore, it balances training stability and dynamic rectification (see Appendix G.4).

6. Experiments

6.1. Experimental Settings

Benchmarks. The benchmark utilized in our work comprises two components: **(1)** *A synthetic dataset* combining a stochastic autoregressive series with a deterministic trigonometric series to validate the **Paradigm Paradox** (Theorem 2.2), and its generation mathematical mechanism is

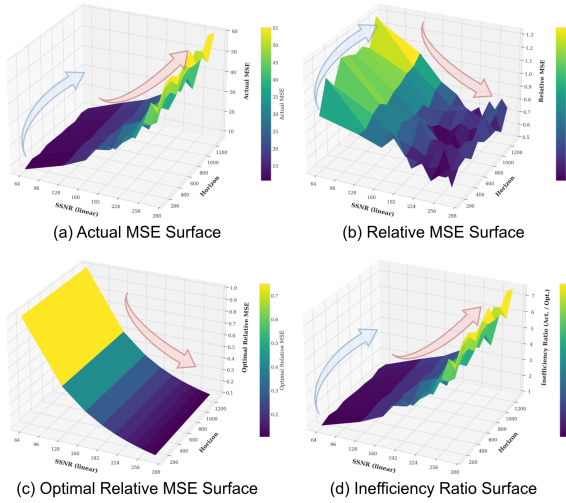


Figure 2: Error surfaces of Transformer with Gaussian distribution innovation. The blue and red arrows indicate the surface variation trend along horizon h and the total SSNR $SSNR_x$, respectively.

detailed in Appendix I.1. Specifically, the non-deterministic SSNR ($SSNR_z = 32$) and variance of innovation noise ($\sigma_\epsilon^2 = 0.25$) are fixed, and the total SSNR ($SSNR_x$) is variable; (2) *Eleven real-world benchmarks* that cover various scenarios, each exhibiting unique characteristics and temporal resolutions, detailed in Appendix I.2. These are used to verify the proposed **Principle Debiasing Program**.

Backbones. Our baselines are categorized into three groups: (1) Transformer-based methods: iTransformer, PatchTST, Pyraformer, FEDformer, Autoformer; (2) MLP-based methods: TimeMixer, TSMixer, DLinear, FrTS; (3) CNN-based methods: TimesNet, MICN; (4) Others: FrDF. We provide detailed descriptions of backbones in Appendix I.3.

Implementation. The baseline models are reproduced using the scripts provided by (Liu et al., 2024) and (Wang et al., 2025b). Our $\mathcal{L}_{Harm, \ell_p}$ is deployed on PatchTST model. Details are provided in Appendix I.4. Notably, we do not use the temporal MSE loss, relying solely on our $\mathcal{L}_{Harm, \ell_p}$.

6.2. Empirical Verification of EOB Theory

To effectively simulate actual data distribution and comprehensively verify the **Paradigm Paradox** and **EOB Theory**, we conducted extreme grid experiments on *5 kinds of foundational deep learning architectures with 6 categories of innovation distributions*. Figure 2 presents the error surfaces of Transformer with Gaussian distribution innovation *w.r.t.* the total SSNR ($SSNR_x$) and forecast horizon (h). Detailed experimental settings are provided in Appendix I.4.1.

Decomposition of Error Dynamics. Figure 2(a) displays

the actual MSE ($MSE_{act.}$), which exhibits a dramatic increase as $SSNR_x$ grows, while also ascending and converging along the forecast horizon h while aligns with the long-term forecasting convergence phenomenon. This behavior is mathematically governed by the relationship between the total variance (σ_x^2) and the relative MSE ($MSE_{rel.}$).

$$MSE_{act.} = \sigma_x^2 \cdot MSE_{rel.} \quad (25)$$

As shown in Figure 2(b), $MSE_{rel.}$ declines monotonically as $SSNR_x$ increases. Intuitively, a higher $SSNR_x$ implies a signal dominated by deterministic patterns, which implies predictability. Consequently, a model with sufficient expressiveness yields a better performance, *i.e.*, lower $MSE_{rel.}$.

Theoretical Optimality. To establish a rigorous baseline, we define the optimal MSE ($MSE^{opt.}$) as the variance of the purely stochastic component, σ_z^2 , representing the irreducible error lower bound of an ideal predictor. Figure 2(c) visualizes the optimal relative MSE ($MSE_{rel.}^{opt.}$) surface which decays rapidly with increasing $SSNR_x$,

$$MSE^{opt.} = SSNR_z \cdot \sigma_\epsilon^2 = \sigma_z^2, \quad (26)$$

$$MSE_{rel.}^{opt.} = \frac{MSE^{opt.}}{\sigma_x^2} = \frac{SSNR_z}{SSNR_x}. \quad (27)$$

Verification of the Paradigm Paradox. The core verification of our EOB theory lies in the *optimization gap* between the actual and optimal performance. To quantify the discrepancy, we define a new metric as follows:

Definition 6.1. (Inefficiency Ratio) For a well-trained model, the *inefficiency ratio* (η) is defined as the ratio of model’s actual MSE to the theoretically optimal MSE:

$$\eta = \frac{MSE_{act.}}{MSE^{opt.}} = \frac{MSE_{act.}}{\sigma_z^2} \quad (28)$$

where σ_z^2 is the variance of unpredictable stochastic part.

Crucially, Figure 2(d) reveals that η grows rapidly as $SSNR_x$ increases, while rises and converges along h . This phenomenon strongly corroborates the insight of **Paradigm Paradox**: as the process becomes more deterministic (higher $SSNR_x$) and theoretically “easier” to predict, the point-wise loss function incurs a progressively larger optimization bias. This forces the model to converge to a solution that is increasingly distant from the theoretical optimum. The elevated EOB signifies a fundamental conflict between the point-wise learning objective and the data’s intrinsic temporal structure. This phenomenon is consistent across diverse foundational deep learning architectures and data distributions (see Appendix J.1 for additional results), demonstrating the *universality* of our EOB theory irrespective of model expressiveness.

Models	$\mathcal{L}_{\text{Harm}, \ell_p}$		FreDF (2025)		TimeMixer (2024)		iTransformer (2024)		PatchTST (2023)		TimesNet (2023)		TSMixer (2023)		DLinear (2023)		FreTS (2023)		MICN (2023)		Pyraformer (2022)		FEDformer (2022)		Autoformer (2021)	
Metrics	MSE	MAE	MSE	MAE	MSE	MAE	MSE	MAE	MSE	MAE	MSE	MAE	MSE	MAE	MSE	MAE	MSE	MAE	MSE	MAE	MSE	MAE	MSE	MAE	MSE	MAE
ETTh1	0.433	0.426	<u>0.445</u>	<u>0.439</u>	0.455	0.443	0.461	0.453	0.454	0.450	0.475	0.464	0.630	0.590	0.461	0.457	0.480	0.468	0.556	0.524	0.893	0.735	0.446	0.460	0.506	0.492
ETTh2	0.371	0.393	<u>0.377</u>	<u>0.400</u>	0.388	0.408	0.390	0.412	0.383	0.409	0.420	0.430	1.613	1.048	0.577	0.528	0.542	0.510	0.570	0.521	2.994	1.441	0.427	0.444	0.434	0.450
ETTm1	0.393	0.390	0.400	0.402	<u>0.385</u>	<u>0.399</u>	0.414	0.414	<u>0.390</u>	0.403	0.407	0.416	0.531	0.514	0.410	0.412	0.419	0.424	0.401	0.428	0.708	0.606	0.442	0.453	0.601	0.521
ETTm2	0.279	0.320	0.280	<u>0.321</u>	<u>0.278</u>	0.325	0.291	0.335	0.288	0.333	0.295	0.334	0.935	0.732	0.356	0.405	0.345	0.394	0.350	0.394	1.494	0.851	0.305	0.348	0.313	0.357
ECL	0.203	0.289	0.171	0.260	0.243	0.347	<u>0.176</u>	<u>0.267</u>	0.208	0.296	0.201	0.302	0.243	0.347	0.266	0.362	0.210	0.299	0.216	0.326	0.322	0.406	0.232	0.341	0.253	0.356
Traffic	0.489	0.296	0.421	<u>0.279</u>	0.503	0.310	<u>0.422</u>	<u>0.282</u>	0.491	0.316	0.625	0.333	0.566	0.385	0.694	0.430	0.554	0.348	0.543	0.320	0.697	0.396	0.620	0.387	0.641	0.401
Weather	0.257	0.273	0.259	0.279	<u>0.245</u>	<u>0.275</u>	0.260	0.281	0.262	0.288	<u>0.244</u>	0.304	0.266	0.317	0.255	0.299	0.267	0.316	0.286	0.348	0.314	0.364	0.350	0.388		
Exchange	0.372	0.409	0.416	0.442	0.369	<u>0.407</u>	<u>0.367</u>	0.411	0.378	0.413	0.440	0.455	0.937	0.724	0.295	0.406	0.377	0.426	0.526	0.531	1.328	0.930	0.509	0.496	0.519	0.506
BE	0.304	0.315	0.335	<u>0.319</u>	0.351	0.352	0.328	0.327	0.313	0.324	0.316	0.326	0.420	0.418	0.375	0.379	0.347	0.352	0.297	0.320	0.350	0.364	0.308	0.333	0.371	0.379
FR	0.287	0.293	0.345	<u>0.300</u>	0.347	0.333	0.344	0.304	<u>0.299</u>	0.305	0.324	0.316	0.405	0.396	0.365	0.367	0.330	0.335	0.313	0.311	0.364	0.359	0.305	0.323	0.379	0.368
PJM	0.311	0.373	0.336	0.389	0.304	0.374	0.305	0.374	0.317	0.384	0.335	0.397	0.334	0.414	0.333	0.407	0.313	0.392	0.264	0.353	<u>0.271</u>	<u>0.364</u>	0.316	0.397	0.366	0.433

Table 1: **The Comprehensive Results on the Long-term Forecasting Task.** **Bold** typeface and underlined text represent the champion and runner-up performance, respectively.

Models	TimeMixer				iTransformer				PatchTST				TimesNet				DLinear					
	$\mathcal{L}_{\text{Harm}, \ell_1}$		$\mathcal{L}_{\text{TMSE}}$		$\mathcal{L}_{\text{Harm}, \ell_1}$		$\mathcal{L}_{\text{TMSE}}$		$\mathcal{L}_{\text{Harm}, \ell_1}$		$\mathcal{L}_{\text{TMSE}}$		$\mathcal{L}_{\text{Harm}, \ell_1}$		$\mathcal{L}_{\text{TMSE}}$		$\mathcal{L}_{\text{Harm}, \ell_1}$		$\mathcal{L}_{\text{TMSE}}$			
Metrics	MSE	MAE	MSE	MAE	MSE	MAE	MSE	MAE	MSE	MAE	MSE	MAE	MSE	MAE	MSE	MAE	MSE	MAE	MSE	MAE	MSE	MAE
ETTh1	96	0.381	0.389	0.382	0.399	0.376	0.394	0.393	0.408	0.379	0.389	0.382	0.400	0.412	0.421	0.412	0.428	0.390	0.403	0.396	0.411	
	192	0.430	0.417	0.437	0.430	0.428	0.421	0.447	0.440	0.427	0.419	0.430	0.433	0.450	0.439	0.457	0.453	0.444	0.438	0.446	0.442	
	336	0.485	0.446	0.485	0.452	0.479	0.441	0.489	0.463	0.464	0.438	0.474	0.460	0.508	0.472	0.506	0.479	0.480	0.456	0.488	0.466	
	720	0.495	0.466	0.518	0.488	0.476	0.475	0.514	0.499	0.460	0.460	0.529	0.508	0.510	0.489	0.523	0.498	0.494	0.495	0.512	0.510	
	Avg	0.448	0.430	0.455	0.443	0.440	0.433	0.461	0.453	0.433	0.426	0.454	0.450	0.470	0.455	0.475	0.464	0.452	0.448	0.461	0.457	
ETTm1	96	0.313	0.342	0.322	0.360	0.327	0.353	0.349	0.379	0.326	0.353	0.327	0.367	0.327	0.359	0.334	0.375	0.340	0.360	0.355	0.379	
	192	0.365	0.368	0.365	0.385	0.378	0.376	0.388	0.397	0.373	0.377	0.371	0.391	0.375	0.385	0.389	0.403	0.381	0.380	0.389	0.396	
	336	0.394	0.390	0.395	0.407	0.420	0.408	0.424	0.420	0.407	0.398	0.399	0.408	0.409	0.409	0.417	0.423	0.412	0.402	0.419	0.418	
	720	0.458	0.429	0.458	0.444	0.490	0.448	0.494	0.459	0.465	0.432	0.460	0.446	0.491	0.454	0.490	0.461	0.472	0.439	0.477	0.454	
	Avg	0.383	0.382	0.385	0.399	0.404	0.396	0.414	0.414	0.393	0.390	0.403	0.401	0.402	0.407	0.416	0.401	0.395	0.410	0.412		

Table 2: **Plug-and-play Experiments of Harmonized ℓ_1 Norm.** **Bold** typeface denotes the champion performance.

6.3. Overall Performance Analysis

Table 1 presents the comprehensive evaluation of proposed loss function deployed on PatchTST against a wide array of SOTA baselines on long-term forecasting tasks. As evidenced by the results, our Harmonized ℓ_p Norm framework consistently achieves superior performance, securing the champion (bold) or runner-up (underlined) position across the majority of datasets and prediction horizons against the SOTA Transformer-, MLP-, and CNN-based algorithms. We argue that although $\mathcal{L}_{\text{Harm}, \ell_p}$ does not achieve the optimal performance in some dataset, but it achieves significant improvement compared with basis model PatchTST.

6.4. Ablation Studies on Optimization Objectives

To verify the effectiveness and universality of our proposed Principled Debiasing Program, we conducted ablation experiments by replacing the standard Temporal Mean Squared Error ($\mathcal{L}_{\text{TMSE}}$) with our proposed Harmonized ℓ_1 Norm ($\mathcal{L}_{\text{Harm}, \ell_1}$), while the former serves as the default training objective for the vast majority of models. As evidenced

by quantitative results are summarized in Table 2, models trained with our $\mathcal{L}_{\text{Harm}, \ell_1}$ consistently outperform those trained with $\mathcal{L}_{\text{TMSE}}$ across almost all datasets, horizons, and architectures, showing a consist performance improvement regardless of the underlying model structure.

7. Conclusion

This work shifts the focus from network expressiveness to the fundamental training paradigm. By scrutinizing the point-wise i.i.d. assumption through a rigorous information-theoretic lens, we formalized the **Optimization Bias**, unveiled the **Paradigm Paradox**, and derived the **unified closed-form quantification** of the non-deterministic EOB. These insights motivated a **Principled Debiasing Program**, which we empirically validated to surpass standard baselines using temporal MSE. Ultimately, we hope to dispel *the haze of AI alchemy* and and nurture its sustainable growth from the ground up.

References

Bao, W., Cao, Y., Yang, Y., Che, H., Huang, J., and Wen, S. Data-driven stock forecasting models based on neural networks: A review. *Information Fusion*, 113:102616, 2025.

Cai, R., Gao, W., Peng, L., Lu, Z., Zhang, K., and Liu, Y. Debiased contrastive learning with supervision guidance for industrial fault detection. *IEEE Transactions on Industrial Informatics*, 20(11):12814–12825, 2024.

Chen, P., ZHANG, Y., Cheng, Y., Shu, Y., Wang, Y., Wen, Q., Yang, B., and Guo, C. Pathformer: Multi-scale transformers with adaptive pathways for time series forecasting. In *The Twelfth International Conference on Learning Representations*, 2024a.

Chen, X., Li, X., Liu, B., and Li, Z. Biased temporal convolution graph network for time series forecasting with missing values. In *The Twelfth International Conference on Learning Representations*, 2024b.

Cheng, R., Jia, X., Li, Q., Xing, R., Huang, J., Zheng, Y., and Xie, Z. FAT: Frequency-aware pretraining for enhanced time-series representation learning. In *Proceedings of the 31st ACM SIGKDD Conference on Knowledge Discovery and Data Mining V.2*, KDD ’25, pp. 310–321, 2025.

Crabbé, J., Huynh, N., Stanczuk, J. P., and Van Der Schaar, M. Time series diffusion in the frequency domain. In *Proceedings of the 41st International Conference on Machine Learning*, volume 235 of *Proceedings of Machine Learning Research*, pp. 9407–9438, 2024.

Cramér, H. *Mathematical Methods of Statistics*, volume 9 of *Princeton Mathematical Series*. Princeton University Press, 1946.

Donghao, L. and Xue, W. ModernTCN: A modern pure convolution structure for general time series analysis. In *The Twelfth International Conference on Learning Representations*, 2024.

Ekambaram, V., Jati, A., Nguyen, N., Sinthong, P., and Kalagnanam, J. TSMixer: Lightweight mlp-mixer model for multivariate time series forecasting. In *Proceedings of the 29th ACM SIGKDD Conference on Knowledge Discovery and Data Mining*, KDD ’23, pp. 459–469, 2023.

Jin, M., Koh, H. Y., Wen, Q., Zambon, D., Alippi, C., Webb, G. I., King, I., and Pan, S. A survey on graph neural networks for time series: Forecasting, classification, imputation, and anomaly detection. *IEEE Transactions on Pattern Analysis and Machine Intelligence*, 46(12):10466–10485, 2024a.

Jin, M., Wang, S., Ma, L., Chu, Z., Zhang, J. Y., Shi, X., Chen, P.-Y., Liang, Y., Li, Y.-F., Pan, S., and Wen, Q. Time-LLM: Time series forecasting by reprogramming large language models. In *The Twelfth International Conference on Learning Representations*, 2024b.

Jin, M., Zhang, Y., Chen, W., Zhang, K., Liang, Y., Yang, B., Wang, J., Pan, S., and Wen, Q. Position: What can large language models tell us about time series analysis. In *Proceedings of the 41st International Conference on Machine Learning*, volume 235, pp. 22260–22276, 2024c.

Kong, Y., Wang, Z., Nie, Y., Zhou, T., Zohren, S., Liang, Y., Sun, P., and Wen, Q. Unlocking the power of lstm for long term time series forecasting. *Proceedings of the AAAI Conference on Artificial Intelligence*, 39(11):11968–11976, 2025.

Kudrat, D., Xie, Z., Sun, Y., Jia, T., and Hu, Q. Patch-wise structural loss for time series forecasting. In *Proceedings of the 42nd International Conference on Machine Learning*, volume 267, pp. 31841–31859, 2025.

Lago, J., Marcjasz, G., De Schutter, B., and Weron, R. Forecasting day-ahead electricity prices: A review of state-of-the-art algorithms, best practices and an open-access benchmark. *Applied Energy*, 293:116983, 2021. ISSN 0306-2619.

Lai, G., Chang, W.-C., Yang, Y., and Liu, H. Modeling long- and short-term temporal patterns with deep neural networks. In *The 41st International ACM SIGIR Conference on Research & Development in Information Retrieval*, SIGIR ’18, pp. 95–104, 2018.

Li, J., Yu, Z., Du, Z., Zhu, L., and Shen, H. T. A comprehensive survey on source-free domain adaptation. *IEEE Transactions on Pattern Analysis and Machine Intelligence*, 46(08):5743–5762, 2024.

Liu, S., Yu, H., Liao, C., Li, J., Lin, W., Liu, A. X., and Dustdar, S. Pyraformer: Low-complexity pyramidal attention for long-range time series modeling and forecasting. In *International Conference on Learning Representations*, 2022.

Liu, Y., Hu, T., Zhang, H., Wu, H., Wang, S., Ma, L., and Long, M. iTransformer: Inverted transformers are effective for time series forecasting. In *The Twelfth International Conference on Learning Representations*, 2024.

Nie, Y., Nguyen, N. H., Sinthong, P., and Kalagnanam, J. A time series is worth 64 words: Long-term forecasting with transformers. In *The Eleventh International Conference on Learning Representations*, 2023.

Qiu, X., Hu, J., Zhou, L., Wu, X., Du, J., Zhang, B., Guo, C., Zhou, A., Jensen, C. S., Sheng, Z., and Yang, B. TFB: Towards comprehensive and fair benchmarking of time series forecasting methods. *Proc. VLDB Endow.*, 17(9): 2363–2377, 2024.

Qiu, X., Wu, X., Cheng, H., Liu, X., Guo, C., Hu, J., and Yang, B. DBLoss: Decomposition-based loss function for time series forecasting. In *NeurIPS*, 2025.

Rasul, K., Seward, C., Schuster, I., and Vollgraf, R. Autoregressive denoising diffusion models for multivariate probabilistic time series forecasting. In *Proceedings of the 38th International Conference on Machine Learning*, volume 139 of *Proceedings of Machine Learning Research*, pp. 8857–8868, 2021.

Ross, S. M. *Introduction to Probability Models (13th Edition)*. Academic Press, 2023.

Vaswani, A., Shazeer, N., Parmar, N., Uszkoreit, J., Jones, L., Gomez, A. N., Kaiser, L. u., and Polosukhin, I. Attention is all you need. In *Advances in Neural Information Processing Systems*, volume 30, 2017.

Wang, H., Peng, J., Huang, F., Wang, J., Chen, J., and Xiao, Y. MICN: Multi-scale local and global context modeling for long-term series forecasting. In *The Eleventh International Conference on Learning Representations*, 2023.

Wang, H., Pan, L., Chen, Z., Chen, X., Dai, Q., Wang, L., Li, H., and Lin, Z. Time-o1: Time-series forecasting needs transformed label alignment, 2025a.

Wang, H., Pan, L., Shen, Y., Chen, Z., Yang, D., Yang, Y., Zhang, S., Liu, X., Li, H., and Tao, D. FreDF: Learning to forecast in the frequency domain. In *The Thirteenth International Conference on Learning Representations*, 2025b.

Wang, S., Wu, H., Shi, X., Hu, T., Luo, H., Ma, L., Zhang, J. Y., and ZHOU, J. Timemixer: Decomposable multi-scale mixing for time series forecasting. In *The Twelfth International Conference on Learning Representations*, 2024.

Wang, S., LI, J., Shi, X., Ye, Z., Mo, B., Lin, W., Shengtong, J., Chu, Z., and Jin, M. Timemixer++: A general time series pattern machine for universal predictive analysis. In *The Thirteenth International Conference on Learning Representations*, 2025c.

Wu, H., Xu, J., Wang, J., and Long, M. Autoformer: Decomposition transformers with auto-correlation for long-term series forecasting. In *Advances in Neural Information Processing Systems*, volume 34, pp. 22419–22430, 2021.

Wu, H., Hu, T., Liu, Y., Zhou, H., Wang, J., and Long, M. Timesnet: Temporal 2d-variation modeling for general time series analysis. In *The Eleventh International Conference on Learning Representations*, 2023.

Xu, Z., Zeng, A., and Xu, Q. FITS: Modeling time series with \$10k\$ parameters. In *The Twelfth International Conference on Learning Representations*, 2024.

Yang, R., Cao, L., Yang, J., and Jianxun, L. Rethinking fourier transform from a basis functions perspective for long-term time series forecasting. In *The Thirty-eighth Annual Conference on Neural Information Processing Systems*, 2024.

Yi, K., Zhang, Q., Fan, W., Wang, S., Wang, P., He, H., An, N., Lian, D., Cao, L., and Niu, Z. Frequency-domain MLPs are more effective learners in time series forecasting. In *Advances in Neural Information Processing Systems*, volume 36, pp. 76656–76679, 2023a.

Yi, K., Zhang, Q., Fan, W., Wang, S., Wang, P., He, H., An, N., Lian, D., Cao, L., and Niu, Z. Frequency-domain MLPs are more effective learners in time series forecasting. In *Thirty-seventh Conference on Neural Information Processing Systems*, 2023b.

Yi, K., Zhang, Q., Fan, W., Cao, L., Wang, S., He, H., Long, G., Hu, L., Wen, Q., and Xiong, H. A survey on deep learning based time series analysis with frequency transformation. In *Proceedings of the 31st ACM SIGKDD Conference on Knowledge Discovery and Data Mining V.2*, KDD ’25, pp. 6206–6215, 2025.

Zeng, A., Chen, M., Zhang, L., and Xu, Q. Are transformers effective for time series forecasting? *Proceedings of the AAAI Conference on Artificial Intelligence*, 37(9), 2023.

Zhang, K., Wen, Q., Zhang, C., Cai, R., Jin, M., Liu, Y., Zhang, J. Y., Liang, Y., Pang, G., Song, D., and Pan, S. Self-supervised learning for time series analysis: Taxonomy, progress, and prospects. *IEEE Transactions on Pattern Analysis and Machine Intelligence*, 46(10):6775–6794, 2024.

Zhang, X., Huang, Z., Wu, Y., Lu, X., Qi, E., Chen, Y., Xue, Z., Wang, Q., Wang, P., and Wang, W. Multi-period learning for financial time series forecasting. In *Proceedings of the 31st ACM SIGKDD Conference on Knowledge Discovery and Data Mining V.1*, KDD ’25, pp. 2848–2859, 2025.

Zhong, S., Ruan, W., Jin, M., Li, H., Wen, Q., and Liang, Y. Time-VLM: Exploring multimodal vision-language models for augmented time series forecasting. In *Forty-second International Conference on Machine Learning*, 2025.

Zhou, H., Zhang, S., Peng, J., Zhang, S., Li, J., Xiong, H., and Zhang, W. Informer: Beyond efficient transformer for long sequence time-series forecasting. *Proceedings of the AAAI Conference on Artificial Intelligence*, 35(12):11106–11115, 2021.

Zhou, T., Ma, Z., Wen, Q., Wang, X., Sun, L., and Jin, R. FEDformer: Frequency enhanced decomposed transformer for long-term series forecasting. In *Proceedings of the 39th International Conference on Machine Learning*, 2022.

Ziyin, L., Hartwig, T., and Ueda, M. Neural networks fail to learn periodic functions and how to fix it. In *Advances in Neural Information Processing Systems*, volume 33, pp. 1583–1594, 2020.

Appendix

Table of Appendix Contents

A Proof of Theorem 2.1 (Bounds on Expectation of Optimization Bias)	13
A.1 Part 1: Proof of $I(z_{1:T}) \leq I(x_{1:T})$	13
A.2 Part 2: Proof of $I(x_{1:T}) \leq I(v_{1:T})$	13
B Proof of Proposition 2.3 (Quantification of Non-deterministic EOB via $AR(p)$)	15
C Relationship Between SSNR and Classical SNR	16
D Quantification of Non-deterministic EOB via Non-Parametric Multivariate Gaussian Model	17
D.1 Proof of Proposition 2.5 (Quantification of Non-deterministic EOB via MGM)	17
D.2 Alignment of the General Optimization Bias Formulas	18
D.3 Proofs of Lemma D.1 and Lemma D.2	19
E Non-linear Modeling of Non-deterministic EOB	22
F Discussion	23
F.1 Bridge between EOB and Model Performance	23
F.2 Unified Reinterpretation of Time Series Analysis Tasks	23
F.3 Theoretical Limitations and Future Development	26
G Characteristic Analysis of DFT, DWT, and Harmonized ℓ_p Norm	27
G.1 Characteristic of Discrete Fourier Transform	27
G.2 Characteristic of Discrete Wavelet Transform	27
G.3 Duality of Gradient Flaws in ℓ_p Norms	28
G.4 Statistical Analysis of Harmonized ℓ_p Norm	28
H Gradient Analysis of Discrete Fourier Transform	31
H.1 Point-wise loss function based on ℓ_2 Norm	31
H.2 Point-wise loss function based on ℓ_1 Norm	32
I Experimental Settings	34
I.1 Synthetic Dataset Generation Mathematical Mechanism	34
I.2 Real-world Benchmark Description	35
I.3 Backbone Description	36
I.4 Implementation Details	37
J Experimental Settings	40
J.1 Empirical Verification of EOB Theory	40
J.2 Long-term Forecasting	40

A. Proof of Theorem 2.1 (Bounds on Expectation of Optimization Bias)

The proof of bounds of expectation of optimization bias is divided into two parts, corresponding to the left and right inequalities. We use the definition of entropy $H(a_t)$, mutual information $I(a_t; a_{1:t-1})$ and $I(a_{1:T})$:

$$H(a_t) = \mathbb{E}[-\log p(a_t)], \quad H(a_t|a_{1:t-1}) = \mathbb{E}[-\log p(a_t|a_{1:t-1})], \quad (29)$$

$$I(a_t; a_{1:t-1}) = \mathbb{E} \left[\log \frac{p(a_t|a_{1:t-1})}{p(a_t)} \right] = H(a_t) - H(a_t|a_{1:t-1}), \quad (30)$$

$$I(a_{1:T}) = \sum_{t=2}^T I(a_t; a_{1:t-1}). \quad (31)$$

The proof is based on the following **basic assumptions**:

- (1) Determination: the deterministic component v_t is perfectly predictable from its past, *i.e.*, $v_t = f(v_{1:t-1})$, such that $p(v_t|v_{1:t-1})$ is a Dirac delta function $\delta(x)$, and $H(v_t|v_{1:t-1}) = -\infty$.
- (2) Independence: The processes $\{v_t\}$ and $\{z_t\}$ is independent.
- (3) Information Equivalence: The information contained in the history $x_{1:t-1}$ is equivalent to the information contained in $\{v_{1:t-1}, z_{1:t-1}\}$.

Then the theorem is equivalent to the inequality about mutual information $I(z_t)$, $I(x_t)$, and $I(v_t)$:

$$I(z_{1:T}) \leq I(x_{1:T}) \leq I(v_{1:T}). \quad (32)$$

A.1. Part 1: Proof of $I(z_{1:T}) \leq I(x_{1:T})$

To prove this, we show that $I(z_t; z_{1:t-1}) \leq I(x_t; x_{1:t-1})$ for any $t \in [2, T]$.

First, we establish that the conditional entropy of x_t given its past is equal to the conditional entropy of z_t given its past.

$$\begin{aligned} H(x_t|x_{1:t-1}) &= H(v_t + z_t|x_{1:t-1}) && \text{(By Decomposition)} \\ &= H(v_t + z_t|v_{1:t-1}, z_{1:t-1}) && \text{(By Condition 3: Information Equivalence)} \\ &= H(z_t|v_{1:t-1}, z_{1:t-1}) && \text{(By Condition 1: Determination)} \\ &= H(z_t|z_{1:t-1}) && \text{(By Condition 2: Independence)} \end{aligned} \quad (33)$$

Next, we compare the marginal entropy of x_t and z_t .

$$\begin{aligned} H(x_t) &= H(v_t + z_t) && \text{(By Decomposition)} \\ &\geq H(z_t) && \text{(By Condition 2: Independence)} \end{aligned} \quad (34)$$

We now compare the mutual information terms:

$$\begin{aligned} I(x_t; x_{1:t-1}) - I(z_t; z_{1:t-1}) &= [H(x_t) - H(x_t|x_{1:t-1})] - [H(z_t) - H(z_t|z_{1:t-1})] \\ &= H(x_t) - H(z_t) \\ &\geq 0. \end{aligned} \quad (35)$$

Thus, $I(x_t; x_{1:t-1}) \geq I(z_t; z_{1:t-1})$. Summing over $t = 2$ to T yields $I(x_{1:T}) \geq I(z_{1:T})$.

A.2. Part 2: Proof of $I(x_{1:T}) \leq I(v_{1:T})$

We analyze the mutual information of the deterministic component $\{v_t\}$:

$$I(v_t; v_{1:t-1}) = H(v_t) - H(v_t|v_{1:t-1}). \quad (36)$$

By Condition 1 (Determination), the process is perfectly predictable, so its conditional entropy is $H(v_t|v_{1:t-1}) = -\infty$. Meanwhile, assuming $\{v_t\}$ is not a fixed constant, its marginal entropy $H(v_t)$ is a finite value. Therefore, the mutual information for a single step is:

$$I(v_t; v_{1:t-1}) = H(v_t) - (-\infty) = \infty. \quad (37)$$

The total correlation is a sum of these terms, which is also infinite:

$$I(v_{1:T}) = \sum_{t=2}^T I(v_t; v_{1:t-1}) = \infty. \quad (38)$$

We analyze the mutual information of the mixed process $\{x_t\}$:

$$I(x_t; x_{1:t-1}) = H(x_t) - H(x_t|x_{1:t-1}). \quad (39)$$

From Eq. (33), we proved $H(x_t|x_{1:t-1}) = H(z_t|z_{1:t-1})$. Because $\{z_t\}$ is a purely non-deterministic process, it has an innovation component with non-zero variance. This means its conditional entropy $H(z_t|z_{1:t-1})$ is a finite value (and strictly $> -\infty$). The marginal entropy $H(x_t)$ is also assumed to be finite for a non-pathological process. Therefore, $I(x_t; x_{1:t-1})$ is the difference between two finite numbers, and is itself finite. The total correlation $I(x_{1:T})$ is a sum of finite terms, which is also finite.

Since $I(x_{1:T})$ is finite and $I(v_{1:T})$ is infinite, the inequality $I(x_{1:T}) \leq I(v_{1:T})$ trivially holds.

Q.E.D.

Notion: The theoretical infinite upper bound of EOB derived from pure deterministic components exists solely as an abstraction. In practice, this bound is constrained by inevitable background noise during data sampling and the finite precision of numerical computing.

B. Proof of Proposition 2.3 (Quantification of Non-deterministic EOB via $AR(p)$)

For $AR(p)$ process, we can specify the exact conditional and marginal distributions required to calculate \mathcal{B}_z :

- **Conditional Distribution:** The distribution of x_t given its past is determined directly by the model's structure. Due to the Markov property of $AR(p)$ model, this simplifies to conditional only on the p preceding time steps.

$$p(z_t|z_{1:t-1}) \sim \mathcal{N}(\mu_t, \sigma_t^2) \quad (40)$$

where $\mu_t = c + \sum_{i=1}^p \phi_i z_{t-i}$ and $\sigma_t^2 = \sigma_\epsilon^2$.

- **Marginal Distribution:** For a stationary $AR(p)$ process, the unconditional distribution of any observation z_t is also Gaussian, with a constant mean and variance.

$$p(z_t) \sim \mathcal{N}(\mu, \sigma^2), \quad \text{where } \mu = \frac{c}{1 - \sum_{i=1}^p \phi_i}. \quad (41)$$

The marginal variance, $\sigma_z^2 = \text{Var}(z_t)$, is determined by the model's parameters $(\phi_i, \sigma_\epsilon^2)$ via the *Yule-Walker Equations*:

$$\sigma_z^2 = \frac{\sigma_\epsilon^2}{1 - \sum_{i=1}^p \phi_i \rho_i} \quad (42)$$

where $\rho_i = \gamma_i / \gamma_0$ is the autocorrelation function at lag i and depends on the ϕ_i in a complex way.

The summation starts from $t = p + 1$ as this is the first time point for which the conditional distribution $p(z_t|z_{1:t-1})$ is fully defined by the p preceding observations, simplifying the analysis by focusing on the steady-state behavior of the process.

Substituting these Gaussian PDFs into the definition of \mathcal{B}_z (Eq. (3)), we obtain:

$$\begin{aligned} \mathcal{B}_z &= \sum_{t=p+1}^T \log \frac{p(z_t|z_{1:t-1})}{p(z_t)} \\ &= \sum_{t=p+1}^T \left[\frac{1}{2} \log \frac{\sigma_z^2}{\sigma_t^2} - \frac{(z_t - \mu_t)^2}{2\sigma_t^2} + \frac{(z_t - \mu)^2}{2\sigma_z^2} \right] \\ &= \sum_{t=p+1}^T \left[\frac{1}{2} \log \frac{\sigma_z^2}{\sigma_\epsilon^2} - \frac{\epsilon_t^2}{2\sigma_\epsilon^2} + \frac{(z_t - \mu)^2}{2\sigma_z^2} \right]. \end{aligned} \quad (43)$$

The expected optimization bias, $\mathbb{E}[\mathcal{B}_z]$, reveals the average magnitude of this systemic error. The expectation of the fluctuation term cancel out, since $\mathbb{E}[(z_t - \mu)^2] = \text{Var}(z_t) = \sigma_z^2$ and $\mathbb{E}[\epsilon_t^2] = \sigma_\epsilon^2$. This leaves a remarkably clean result:

$$\mathbb{E}[\mathcal{B}] = \frac{T-p}{2} \log \frac{\sigma_z^2}{\sigma_\epsilon^2} = \frac{T-p}{2} \log \frac{1}{1 - \sum_{i=1}^p \phi_i \rho_i}. \quad (44)$$

C. Relationship Between SSNR and Classical SNR

This appendix clarifies the precise relationship between the Structural Signal-to-Noise Ratio (*SSNR*), as defined in our main analysis, and the classical Signal-to-Noise Ratio (*SNR*) widely used in information theory and signal processing.

The classical SNR quantifies the ratio of the power of a pure signal to the power of confounding noise. For a zero-mean process, power is equivalent to variance. Given a pure signal component \hat{S} with variance $\hat{\sigma}^2 = \mathbb{E}[\hat{S}^2]$ and an additive noise component ϵ with variance $\sigma_\epsilon^2 = \mathbb{E}[\epsilon^2]$, the classical SNR is defined as:

$$SNR = \frac{P_{\text{signal}}}{P_{\text{noise}}} = \frac{\hat{\sigma}^2}{\sigma_\epsilon^2}. \quad (45)$$

In our framework, the observed time series S is modeled as a composite of the pure, structured signal \hat{S} and the irreducible innovation noise ϵ , such that $S = \hat{S} + \epsilon$. A standard assumption is that the signal \hat{S} and the noise ϵ are statistically independent, which implies they are orthogonal ($\mathbb{E}[\hat{S}\epsilon] = 0$). This orthogonality allows the variance of the observed signal, σ_z^2 , to be decomposed as a sum of the signal and noise variances:

$$\begin{aligned} \sigma_z^2 &= \text{Var}(S) = \mathbb{E}[S^2] \\ &= \mathbb{E}[\hat{S}^2] + 2\mathbb{E}[\hat{S}\epsilon] + \mathbb{E}[\epsilon^2] \\ &= \hat{\sigma}^2 + \sigma_\epsilon^2. \end{aligned} \quad (46)$$

Our SSNR is defined as the ratio of the total variance of the observed process to the variance of its innovation noise $SSNR = \sigma_z^2/\sigma_\epsilon^2$. This definition is adopted for its mathematical convenience and direct utility in deriving the expected optimization bias. Using the variance decomposition above, we can establish a simple algebraic bridge between our SSNR and the classical SNR:

$$SSNR = \frac{\hat{\sigma}^2}{\sigma_\epsilon^2} + \frac{\sigma_\epsilon^2}{\sigma_\epsilon^2} = SNR + 1. \quad (47)$$

Thus, the SSNR used in our work is precisely the classical SNR plus one. This formulation is analytically elegant and simplifies the expression of our main theoretical results.

D. Quantification of Non-deterministic EOB via Non-Parametric Multivariate Gaussian Model

D.1. Proof of Proposition 2.5 (Quantification of Non-deterministic EOB via MGM)

D.1.1. NON-PARAMETRIC OPTIMIZATION BIAS MODELING

The main text provides a closed-form quantification of the expectation of optimization bias using a parametric linear model, the $AR(p)$ process. While this provides a clear and intuitive result linked to $SSNR$, one might question its applicability to the complex, non-linear dynamics captured by modern deep learning models.

To address this issue and establish a more general foundation, we re-derive the expectation of optimization bias under a more general assumption: that any T -dimensional time series sequence z can be modeled as a single sample from a general *Multivariate Gaussian Model*, $z \sim \mathcal{N}(\mu, \Sigma)$. This is a more general linear model assumption than the $AR(p)$ process because it places no constraints on the structure of the covariance matrix Σ .

The non-deterministic optimization bias \mathcal{B}_z is the log-likelihood divergence between the true joint distribution $p(z_{1:T}) = p(z_1) \cdot \prod_{t=2}^T p(z_t|z_{1:t-1})$ and the simplified independent distribution $q(z_{1:T}) = \prod_{t=1}^T p(z_t)$ of assumed by point-wise loss:

$$\mathcal{B}_z = \sum_{t=2}^T \log \frac{p(z_t|z_{1:t-1})}{p(z_t)} = \log \frac{p(z_{1:T})}{q(z_{1:T})} = \log \frac{p(z_{1:T})}{\prod_{t=1}^T p(z_t)} = \log p(z_{1:T}) - \sum_{t=1}^T \log p(z_t). \quad (48)$$

By substituting the log-PDFs for the multivariate and univariate Gaussian distributions, we get:

$$\log p(z_{1:T}) = -\frac{T}{2} \cdot \log(2\pi) - \frac{1}{2} \log |\Sigma| - \frac{1}{2}(z - \mu)^\top \Sigma^{-1}(z - \mu) \quad (49)$$

$$\log p(z_t) = -\frac{1}{2} \cdot \log(2\pi) - \frac{1}{2} \log \sigma_t^2 - \frac{(z_t - \mu_t)^2}{2\sigma_t^2} \quad (50)$$

$$\mathcal{B}_z = -\frac{1}{2} \log |\Sigma| - \frac{1}{2}(z - \mu)^\top \Sigma^{-1}(z - \mu) + \frac{1}{2} \sum_{t=1}^T \log \sigma_t^2 + \frac{1}{2} \sum_{t=1}^T \frac{(z_t - \mu_t)^2}{\sigma_t^2}. \quad (51)$$

Taking the expectation and using the standard results that $\mathbb{E}[(z - \mu)^\top \Sigma^{-1}(z - \mu)] = T$ and $\mathbb{E}[(z_t - \mu_t)^2] = \sigma_t^2$, the quadratic terms cancel, leaving

$$\mathbb{E}[\mathcal{B}_z] = -\frac{1}{2} \left(\log |\Sigma| - \sum_{t=1}^T \log \sigma_t^2 \right) = \frac{1}{2} \log \left(\frac{\prod_{t=1}^T \sigma_t^2}{|\Sigma|} \right). \quad (52)$$

To reveal the core insight, we introduce the correlation matrix R with elements $R_{ij} = \rho_{|i-j|}$, defined by the relationship $\Sigma = D^{1/2} R D^{1/2}$, where $D = \text{diag}(\sigma_1^2, \dots, \sigma_T^2)$ is the diagonal matrix of variances. Taking the determinant, we have:

$$|\Sigma| = |D||R| = \left(\prod_{t=1}^T \sigma_t^2 \right) |R|. \quad (53)$$

Substituting this into the expression for $\mathbb{E}[\mathcal{B}_z]$ yields a remarkably simple and general result:

$$\mathbb{E}[\mathcal{B}_z] = \frac{1}{2} \log \left(\frac{\prod_{t=1}^T \sigma_t^2}{(\prod_{t=1}^T \sigma_t^2) |R|} \right) = -\frac{1}{2} \log |R|. \quad (54)$$

This elegant result shows that the expectation of optimization bias is purely a function of the determinant of the correlation matrix $|R|$. The determinant $|R|$ is a scalar value between 0 (perfect linear dependence) and 1 (complete independence), representing the "volume" of the correlation structure.

D.1.2. LINK WITH SEQUENCE LENGTH AND SSNR

This general result is fully consistent with and provides a deeper foundation for the two key factors: Sequence Length and SSNR, which identified in our main analysis using the $AR(p)$ model. The determinant $|R|$ is an elegantly interconnected representation of them:

- **Connection to Sequence Length (T):** The correlation matrix R is of size $T \times T$. For any time series with non-zero autocorrelation, the determinant $|R|$ is a monotonically decreasing function of its dimension, T . As the sequence lengthens, the cumulative effect of correlation drives $|R|$ exponentially towards zero. Consequently, $\mathbb{E}[\mathcal{B}_z] = -\frac{1}{2} \log |R|$ naturally increases with the sequence length.
- **Connection to SSNR:** The determinant $|R|$ serves as an inverse measure of the total correlation strength within the sequence. A process with a high SSNR is, by definition, highly predictable with strong and persistent autocorrelations. This strong internal structure is reflected in the matrix R (i.e., larger off-diagonal values), causing its determinant $|R|$ to be significantly smaller than that of a less predictable (low SNR) process. A smaller $|R|$ directly corresponds to a larger optimization bias.

Therefore, the expression $\mathbb{E}[\mathcal{B}_z] = -\frac{1}{2} \log |R|$ can be viewed as a more fundamental principle. The intuitive effects of sequence length and structural predictability, which we derived in the parametric $AR(p)$ case, are naturally captured within this single, comprehensive measure.

For the special case of a *covariance-stationary process*, where $\sigma_t^2 = \sigma_z^2$ for all t , the formula becomes:

$$\mathbb{E}[\mathcal{B}] = \frac{T}{2} \log \frac{\sigma_z^2}{|\Sigma|^{1/T}}. \quad (55)$$

This connects back to our $AR(p)$ model analysis, which is a specific instance of a stationary process where the structure of Σ is known, allowing us to derive the relationship with SSNR.

This derivation confirms that the Optimization Bias is not an artifact of the linear $AR(p)$ model but a fundamental property of any correlated (Gaussian) process. It provides a robust theoretical foundation for our claim that point-wise loss is inherently flawed for time series data, regardless of whether the underlying process is modeled as parametric or non-parametric.

D.2. Alignment of the General Optimization Bias Formulas

In this appendix, we derived a general formula for the expectation of optimization bias for any process modeled as a multivariate Gaussian: $\mathbb{E}[\mathcal{B}_z] = -\frac{1}{2} \log |R|$. We now demonstrate that this general result is fully consistent with the formula derived in the main text, $\mathbb{E}[\mathcal{B}_z] = \frac{T-p}{2} \log(\text{SSNR})$, by generalizing our formula.

D.2.1. EQUIVALENCE FOR INFINITE T

We now formally prove the asymptotic equivalence between our two primary results for the expectation of optimization bias: the general, non-parametric formula derived from the multivariate Gaussian model (Eq. (54)), and the simpler, parametric approximation for the $AR(p)$ process (Eq. (7)).

The general formula is $\mathbb{E}[\mathcal{B}_z]_{\text{MGM}} = -\frac{1}{2} \log |R|$. The formula for an $AR(p)$ process is $\mathbb{E}[\mathcal{B}_z]_{\text{AR}} = \frac{T-p}{2} \log(\text{SSNR})$. To prove that these two expressions are asymptotically equivalent, we will show that the limit of their ratio is 1:

$$\lim_{T \rightarrow \infty} \frac{\mathbb{E}[\mathcal{B}_z]_{\text{AR}}}{\mathbb{E}[\mathcal{B}_z]_{\text{MGM}}} = 1. \quad (56)$$

We have:

$$\lim_{T \rightarrow \infty} \frac{\frac{T-p}{2} \log(\text{SSNR})}{-\frac{1}{2} \log |R|} = \lim_{T \rightarrow \infty} \left(1 - \frac{p}{T}\right) \frac{\log(\text{SSNR})}{-\log |R|^{1/T}} = \lim_{T \rightarrow \infty} \frac{\log(\sigma_z^2/\sigma_\epsilon^2)}{\log |R|^{1/T}} = 1. \quad (57)$$

The Lemma D.1 provides the necessary identity to solve this limit, thereby proving the equivalence.

D.2.2. EXACT FORMULA FOR FINITE T

More powerfully, for a finite sequence of length T from a stationary $AR(p)$ process, there exists an exact identity for the determinant of the correlation matrix by Lemma D.2:

$$|R| = |R_p| \cdot \left(\frac{\sigma_\epsilon^2}{\sigma_z^2} \right)^{T-p} = |R_p| \cdot \left(\frac{1}{\text{SSNR}} \right)^{T-p}. \quad (58)$$

By substituting this identity directly into our general bias formula, we obtain the exact expression for the expectation of optimization bias:

$$\begin{aligned}\mathbb{E}[\mathcal{B}_z] &= -\frac{1}{2} \log |R| = -\frac{1}{2} \log \left[|R_p| \cdot \left(\frac{1}{SSNR} \right)^{T-p} \right] \\ &= \frac{T-p}{2} \log(SSNR) - \frac{1}{2} \log |R_p|.\end{aligned}\tag{59}$$

Discussion.

This proposition provides a profound insight into the nature of the expectation of optimization bias. The exact formula reveals that the bias is composed of two distinct parts:

- **A primary term**, $\frac{T-p}{2} \log(SSNR)$, which grows linearly with the sequence length T and is logarithmically proportional to the SSNR. This is identical to the intuitive result derived from $AR(p)$ model.
- **A correction term**, $-\frac{1}{2} \log |R_p|$, which is a constant offset depending only on the first p autocorrelations of the process. For any reasonably long sequence where $T \gg p$ or low memory sequence $|R_p| \rightarrow 1$, this correction term is negligible compared to the primary term.

More generally, the exact optimization bias can be re-expressed as:

$$\mathbb{E}[\mathcal{B}_z] = \frac{T}{2} \log(SSNR) + C(SSNR)\tag{60}$$

where $C(SSNR)$ denotes a constant only relying on SSNR.

D.3. Proofs of Lemma D.1 and Lemma D.2

Lemma D.1. (The Asymptotic Convergence of Autocorrelation Matrix Determinant Geometric Mean) For a covariance-stationary process, let R be its $T \times T$ correlation matrix. As the sequence length T approaches infinity, the geometric mean of the eigenvalues of R , represented by $|R|^{1/T}$, converges to the reciprocal of the SSNR:

$$\lim_{T \rightarrow \infty} |R|^{1/T} = \frac{\sigma_\epsilon^2}{\sigma_z^2} = \frac{1}{SSNR}\tag{61}$$

where ϕ_i are the autoregressive coefficients and ρ_i is the autocorrelation function at lag i .

Proof.

The proof begins with Szegő's First Limit Theorems, a powerful result concerning the determinants of Toeplitz matrix. For a covariance-stationary process, the correlation matrix R is a *Toeplitz matrix*, with elements $R_{ij} = \rho_{|i-j|}$. The theorem connects the asymptotic behavior of the determinant $|R|$ to the power spectral density, $f(\omega)$, of the process:

$$\lim_{T \rightarrow \infty} \frac{1}{T} \log |R| = \frac{1}{2\pi} \int_{-\pi}^{\pi} \log f(\omega) d\omega.\tag{62}$$

For an $AR(p)$ process, the power spectral density is given by:

$$f(\omega) = \frac{\sigma_\epsilon^2}{2\pi \left| 1 - \sum_{k=1}^p \phi_k e^{-ik\omega} \right|^2}.\tag{63}$$

Applying Kolmogorov's Formula, the integral of the log-spectrum for any stationary, non-deterministic process simplifies to the log-ratio of the innovation variance (σ_ϵ^2) to the marginal variance (σ_z^2):

$$\frac{1}{2\pi} \int_{-\pi}^{\pi} \log f(\omega) d\omega = \log \sigma_\epsilon^2 - \log \sigma_z^2 = \log \left(\frac{\sigma_\epsilon^2}{\sigma_z^2} \right).\tag{64}$$

Combining these results, we find the limit:

$$\lim_{T \rightarrow \infty} \log |R|^{1/T} = \log \left(\frac{\sigma_\epsilon^2}{\sigma_z^2} \right). \quad (65)$$

Exponentiating both sides yields the final result:

$$\lim_{T \rightarrow \infty} |R|^{1/T} = \frac{\sigma_\epsilon^2}{\sigma_z^2} = \frac{1}{SSNR}. \quad (66)$$

Q.E.D.

Lemma D.2. (Determinant Decomposition for AR(p) Correlation Matrix) Let $\{x_t\}$ be a stationary AR(p) process with unconditional variance σ_z^2 and innovation variance σ_ϵ^2 . For a sequence of length $T > p$, let R denote the $T \times T$ correlation matrix of the vector (z_1, \dots, z_T) and R_p be the $p \times p$ correlation matrix of the initial p observations (z_1, \dots, z_p) . The determinant of the full correlation matrix is given by:

$$|R| = |R_p| \cdot \left(\frac{\sigma_\epsilon^2}{\sigma_z^2} \right)^{T-p}. \quad (67)$$

Proof.

The proof proceeds by deriving two expressions for the joint log-probability density function (log-PDF) of the sequence $z_{1:T} = (z_1, \dots, z_T)$ under the assumption of a multivariate Gaussian distribution, and then equating terms.

By the chain rule of probability and the Markov property of an AR(p) process, the joint log-PDF can be factored into the log-PDF of the first p observations and the sum of subsequent $T - p$ conditional log-PDFs:

$$\log p(z_{1:T}) = \log p(z_{1:p}) + \sum_{t=p+1}^T \log p(z_t | z_{t-p:t-1}). \quad (68)$$

We can express each term as a Gaussian log-PDF:

- The full series $z := z_{1:T}$ follows a multivariate Gaussian with covariance matrix Σ and mean vector μ . Its log-PDF is:

$$\log p(z_{1:T}) = -\frac{T}{2} \log(2\pi) - \frac{1}{2} \log |\Sigma| - \frac{1}{2} (z - \mu)^\top \Sigma^{-1} (z - \mu). \quad (69)$$

- The initial series $z_p := z_{1:p}$ is a multivariate Gaussian with covariance matrix Σ_p and mean vector μ_p . Its log-PDF is:

$$\log p(z_{1:p}) = -\frac{p}{2} \log(2\pi) - \frac{1}{2} \log |\Sigma_p| - \frac{1}{2} (z_p - \mu_p)^\top \Sigma_p^{-1} (z_p - \mu_p). \quad (70)$$

- Each conditional term $p(z_t | z_{t-p:t-1})$ corresponds to the process's innovation $\epsilon_t = z_t - c - \sum_{i=1}^p \phi_i z_{t-i}$ based on (6), which is a univariate Gaussian with variance σ_ϵ^2 . Its log-PDF is:

$$\log p(z_t | z_{t-p:t-1}) = -\frac{1}{2} \log(2\pi) - \frac{1}{2} \log \sigma_\epsilon^2 - \frac{(z_t - \mu_t)^2}{2\sigma_\epsilon^2}. \quad (71)$$

Substituting in (68):

$$\log |\Sigma| + (z - \mu)^\top \Sigma^{-1} (z - \mu) = \log |\Sigma_p| + (z_p - \mu_p)^\top \Sigma_p^{-1} (z_p - \mu_p) + (T - p) \log \sigma_\epsilon^2 + \sum_{t=p+1}^T \frac{(z_t - \mu_t)^2}{\sigma_\epsilon^2}. \quad (72)$$

Since this equality holds for any realization, the expectation of the left side must equal the expectation of the right side. We have:

$$\begin{cases} \mathbb{E}[(z - \mu)^\top \Sigma^{-1} (z - \mu)] = T \\ \mathbb{E}[(z_p - \mu_p)^\top \Sigma_p^{-1} (z_p - \mu_p)] = p \\ \sum_{t=p+1}^T \mathbb{E}[(z_t - \mu_t)^2 / \sigma_\epsilon^2] = T - p. \end{cases} \quad (73)$$

Plugging these results back into the (72) gives:

$$|\Sigma| = |\Sigma_p| \cdot (\sigma_\epsilon^2)^{T-p}. \quad (74)$$

For a stationary process, the marginal variance σ_z^2 is constant. The covariance matrix Σ and correlation matrix R are related by $\Sigma = \sigma_z^2 R$. Using the determinant property $|\lambda A| = (\lambda)^k |A|$ for a $k \times k$ matrix A .

$$\begin{cases} |\Sigma| = (\sigma_z^2)^T |R| \\ |\Sigma_p| = (\sigma_z^2)^p |R_p|. \end{cases} \quad (75)$$

Substituting these into the covariance identity:

$$|R| = |R_p| \cdot \left(\frac{\sigma_\epsilon^2}{\sigma_z^2} \right)^{T-p}. \quad (76)$$

This can also be expressed using the SSNR ($SSNR = \sigma_z^2 / \sigma_\epsilon^2$):

$$|R| = |R_p| \cdot \left(\frac{1}{SSNR} \right)^{T-p}. \quad (77)$$

Q.E.D.

E. Non-linear Modeling of Non-deterministic EOB

To extend our analysis beyond the linear domain, we now consider non-deterministic processes governed by non-linear dynamics. A canonical approach for modeling such complexity is the **Gaussian Mixture Model (GMM)**, which represents the process distribution as a weighted sum of multiple Gaussian components:

$$p(z) = \sum_{k=1}^K \pi_k \mathcal{N}(z_k | \mu_k, \Sigma_k) = \sum_{k=1}^K \pi_k p(z_k) \quad (78)$$

where $p(z_k)$ represents the k -th Gaussian component and π_k is its corresponding mixture weight.

Directly computing the non-deterministic EOB for a GMM is analytically intractable due to the logarithm-of-sums form, $\log \left(\sum_{k=1}^K \pi_k p(z_k) \right)$, inherent in its log-likelihood. To overcome this obstacle, we reformulate the EOB using the language of information theory, expressing it in terms of differential entropy, defined as $H(x) = \mathbb{E}[-\log p(x)]$.

This approach elegantly recasts the non-deterministic EOB in terms of entropy:

$$\begin{aligned} \mathbb{E}[\mathcal{B}_z] &= \mathbb{E} \left[\log \frac{p(z_{1:T})}{\prod_{t=1}^T p(z_t)} \right] \\ &= \mathbb{E}[\log p(z_{1:T})] - \sum_{t=1}^T \mathbb{E}[\log p(z_t)] \\ &= -H(z_{1:T}) + \sum_{t=1}^T H(z_t). \end{aligned} \quad (79)$$

While the differential entropy of a GMM distribution lacks a close-form solution, it is tightly bounded. Applying *Jensen's Inequality* establishes the standard lower and upper bounds for $H(z)$:

$$\sum_{k=1}^K \pi_k H(z_k) \leq H(z) \leq \sum_{k=1}^K \pi_k H(z_k) + H(\pi) \quad (80)$$

where $H(\pi) = -\sum_{k=1}^K \pi_k \log \pi_k$ is the Shannon entropy of the mixture weights.

$$\begin{cases} -H(z_{1:T}) \geq -\sum_{k=1}^K \pi_k H(z_{k,1:T}) - H(\pi) \\ H(z_t) \geq \sum_{k=1}^K \pi_k H(z_{k,t}). \end{cases} \quad (81)$$

By substituting these entropy bounds into our EOB expression, we can derive a lower bound for the non-deterministic EOB of the GMM process. Assuming stationarity, where the mixture weights π_k are constant over time, we can regroup the terms by their respective components:

$$\begin{aligned} \mathbb{E}[\mathcal{B}_z] &\geq \sum_{k=1}^K \pi_k \left[\sum_{t=1}^T H(z_{k,t}) - H(z_{k,1:T}) \right] - H(\pi) \\ &= \sum_{k=1}^K \pi_k \mathbb{E} \left[\log \frac{p(z_{k,1:T})}{\prod_{t=1}^T p(z_{k,t})} \right] - H(\pi) \\ &= \sum_{k=1}^K \pi_k \mathbb{E}[\mathcal{B}_k] - H(\pi). \end{aligned} \quad (82)$$

F. Discussion

F.1. Bridge between EOB and Model Performance

The connection between our implicit, abstract EOB and explicit evaluation metrics like MSE or MAE is not one of direct equivalence, but of fundamental precondition. We argue that minimizing EOB as a measure of the “pathology” of the optimization landscape is a crucial proxy objective for improving these practical metrics. A high EOB signifies a conflict between the learning objective and the data’s intrinsic temporal structure. This pathological optimization landscape makes it difficult for any model, regardless of its expressive power, to converge to a robust and generalizable solution. Therefore, by minimizing EOB, we are not directly minimizing MSE but are instead creating a more well-posed optimization problem. A lower EOB ensures the learning signal is better aligned with the data’s true generative process, thereby providing a more stable foundation upon which a model can more readily achieve optimal performance on explicit metrics like MSE.

F.2. Unified Reinterpretation of Time Series Analysis Tasks

F.2.1. A MECHANISM-BASED TAXONOMY OF TIME SERIES ANALYSIS

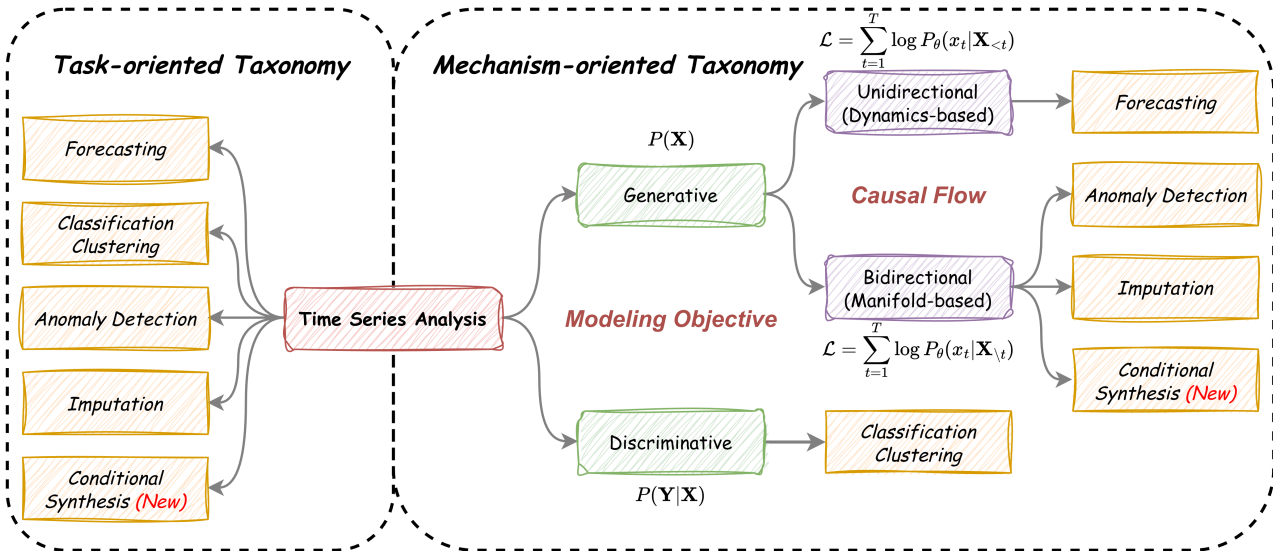


Figure 3: Taxonomies of Time Series Analysis.

The conventional *task-oriented taxonomy* categorizes time series analysis into five distinct silos: forecasting, classification / clustering, anomaly detection, imputation, and emerging conditional synthesis. This categorization, focusing primarily on the downstream applications rather than modeling methodologies, lacks the theoretical granularity to reconcile with emerging paradigms in the era of LLMs, such as conditional generation. To address this limitation, we propose a novel **Mechanism-Oriented Taxonomy** that fundamentally reorganizes the logic of time series analysis based on modeling objective and causal flow.

1. Generative vs. Discriminative: The Modeling Objective

From the perspective of modeling objective, we categorize tasks into *generative* and *discriminative* paradigms.

- **Generative Tasks** aim to approximate the underlying data distribution or the intrinsic pattern of the original series \mathbf{X} , *i.e.*, modeling the joint probability $P(\mathbf{X})$.
- **Discriminative Tasks** function as an information bottleneck processes, establishing decision boundaries to distinguish labels \mathbf{Y} by modeling the conditional probability $P(\mathbf{Y}|\mathbf{X})$.

Consequently, we re-categorize forecasting, anomaly detection, imputation, and the emerging conditional synthesis as **Generative tasks**, while classification / clustering remains **Discriminative**. Notably, although anomaly detection is often treated as a binary classification problem, its mainstream unsupervised formulation relies on learning the density of normal

states and identifying outliers via low likelihood or high reconstruction error. Thus, it essentially follows the generative paradigm.

2. Dynamics vs. Manifold: The Causal Flow

Within the generative paradigm, we further classify tasks based on the directionality of causal flow (*i.e.*, information flow) into two sub-categories: **Unidirectional (Dynamics-based)** and **Bidirectional (Manifold-based)**.

A. Unidirectional Generation (Dynamics-based) This category strictly adheres to the arrow of time, focusing on **Causality** and **Extrapolation**. Dynamics-based models access only unidirectional historical information to model the evolution of states, predicting future trajectories via stochastic process. The representative task is **Forecasting**. The objective is typically formulated as maximizing the autoregressive likelihood:

$$\mathcal{L}_{\text{Uni}} = \sum_{t=1}^T \log P_{\theta}(x_t | \mathbf{X}_{<t}) \quad (83)$$

where $\mathbf{X}_{<t} = \{x_1, \dots, x_{t-1}\}$ represents the historical context *w.r.t.* x_t .

B. Bidirectional Generation (Manifold-based) This category leverages the global context, focusing on **Consistency** and **Interpolation**. Manifold-based models utilizes bidirectional information to capture global statistics and structural correlations. This group encompasses **Imputation**, **Anomaly Detection**, and **Conditional Synthesis**. The objective is formulated as maximizing the composite pseudo-likelihood:

$$\mathcal{L}_{\text{Bi}} = \sum_{t=1}^T \log P_{\theta}(x_t | \mathbf{X}_{\setminus t}) \quad (84)$$

where $\mathbf{X}_{\setminus t} = \{x_1, \dots, x_{t-1}, x_{t+1}, \dots, x_T\}$ is the global context masking the current state x_t .

3. Imputation and Anomaly Detection as Twin Tasks

Under the manifold-based generative group, we posit that **Imputation** and **Anomaly Detection** are theoretically *isomorphic* or *inverse* problems grounded in the same manifold structure \mathcal{M} .

- **Imputation (Projection):** The goal is to project an incomplete observation onto the learned manifold. Specifically, imputation attempts to search for the closest point \hat{x}_t on the manifold \mathcal{M} to replace the missing or observed point:

$$\hat{x}_t \sim P_{\theta}(x | \mathbf{X}_{\setminus t}) \quad (85)$$

$$\hat{x}_t \approx \text{Proj}_{\mathcal{M}}(\mathbf{X}_{\setminus t}). \quad (86)$$

- **Anomaly Detection (Evaluation):** The goal is to measure the deviation of an observed point $\bar{\mathbf{X}}$ from the manifold surface \mathcal{M} . If the likelihood is below a threshold or a distance exceeds error tolerance, the point is deemed abnormal.

$$\mathcal{A}(x_t) = -\log P_{\theta}(x_t | \mathbf{X}_{\setminus t}). \quad (87)$$

Crucially, in this paradigm, the current state x_t **must be masked** during the evaluation phase of anomaly detection. This prevents the trivial solution where the projector $\text{Proj}_{\mathcal{M}}(\cdot)$ learns an identity mapping based solely on current state x_t . Therefore, anomaly detection fundamentally relies on reconstruction capability aligning with imputation task, that one cannot detect deviations from a manifold without first learning to generate valid points upon it.

4. Conditional Synthesis

For the emerging task of conditional synthesis, the target manifold $\bar{\mathcal{M}}$ is jointly determined by the original data distribution \mathcal{D} and external conditions \mathcal{C} (*e.g.*, text prompts or physical parameters). The objective is to sample a personalized trajectory $\bar{\mathbf{X}}$ that resides within this conditional manifold $\bar{\mathcal{M}}$.

$$\bar{\mathbf{X}} \sim P_{\theta}(x | \bar{\mathcal{M}}(\mathcal{D}, \mathcal{C})). \quad (88)$$

F.2.2. SYSTEMATIC REVIEW OF MECHANISM-ORIENTED TAXONOMY VIA EOB THEORY

Regardless of the underlying architecture, in the absence of domain-specific priors, point-wise loss functions based on the i.i.d. assumption (*e.g.*, MSE, MAE, and Cross Entropy) remain the standard constraint for optimization. We conduct a systematic review of time series analysis tasks through the lens of EOB Theory to elucidate the impact of optimization bias.

1. Discriminative Paradigm

The primary objective of the discriminative paradigm is to establish robust decision boundaries for label distinction, typically employing Cross Entropy loss on one-hot encodings.

We approach discriminative paradigm from a sequential perspective. Specifically, a one-hot label vector can be viewed as a discrete sequence composed of orthogonal elements. Unlike generative tasks that require precise value reconstruction, classification focuses on the location of the maximum probability (argmax). Cross entropy loss is also a specific point-wise loss function for probability approximation. Due to the orthogonality of the one-hot distribution, its SSNR is 1, corresponding to the theoretical minimum. This implies that the EOB for the discriminative paradigm is effectively zero. Thus, *the discriminative paradigm is theoretically unbiased and can naturally achieve optimal performance*.

2. Generative Paradigm

In stark contrast to the discriminative paradigm, the generative paradigm aims to model the underlying data distribution $P(\mathbf{X})$ or generate trajectories based on contexts. Here, the optimization target is the time series values themselves, which inherently possess strong temporal correlations and deterministic structures (e.g., trend and periodicity). Consequently, SSNR is significantly greater than 1 ($SSNR \gg 1$). According to Theorem 2.6, the EOB lower bound grows logarithmically with SSNR, implying that *the generative paradigm is inherently biased under point-wise loss functions in temporal domain*. We further analyze this bias across two sub-categories defined in our mechanism-oriented taxonomy.

A. Unidirectional Generation (Dynamics-based)

This category, represented by forecasting, strictly adheres to the causal flow of time by modeling $P(x_t | \mathbf{X}_{})$. This formulation aligns directly with the parametric autoregressive modeling ($AR(p)$) of EOB lower bound derived in Section 2.2.1.

The fundamental objective here is **extrapolation**: leveraging historical dynamics to accurately estimate distributions or deterministic patterns for future states. However, as formalized in the **Paradigm Paradox** (Theorem 2.2), the more deterministic the dynamics (i.e., higher SSNR), the more severely the point-wise independence assumption conflicts with the data structure. Consequently, the loss function forces the model to treat highly correlated steps as independent events, creating a fundamental resistance against learning long-term dependencies. Thus, unidirectional generation suffers from the *Maximum Optimization Bias*, providing a theoretical explanation for why simpler models often fail to capture periodicities despite possessing sufficient expressiveness.

B. Bidirectional Generation (Manifold-based)

This category, encompassing imputation, anomaly detection, and conditional synthesis, leverages global statistics to model $P(x_t | \mathbf{X}_{\setminus t})$. This formulation aligns directly with the non-parametric multivariate Gaussian modeling (MGM) of the EOB lower bound discussed in Section 2.2.2.

Conceptually, these tasks involve projecting data onto a learned manifold or detecting deviations from it, with the optimization target being the reconstruction of masked or corrupted signals. Although masking introduces artificial discontinuity, slightly reducing local correlation, the reconstruction target remains the original high-SSNR signal. The model seeks to restore global consistency via interpolation. However, standard point-wise reconstruction losses (e.g., MSE on masked patches) treat error at each point independently, neglecting the inherent correlations within the error structure itself. Ultimately, despite the availability of the bidirectional context, the optimization landscape remains pathological due to the high SSNR of the target. The bias typically manifests as blurred reconstructions or manifold collapse, as the loss function converges toward the mean behavior favored by the i.i.d. assumption rather than preserving detailed structural integrity.

In the specific case of emerging conditional synthesis, the EOB causes the statistical characteristics of synthesized data to deviate significantly from the constraints imposed by external conditions.

Thus, unlike the unbiased discriminative paradigm, the generative paradigm is fundamentally impacted by the EOB inherent in point-wise loss functions. This theoretical dichotomy provides the rigorous justification for our proposed **Debiasing Program**, establishing it as an essential intervention for generative tasks while remaining optional for discriminative ones.

F.3. Theoretical Limitations and Future Development

We must scrutinize our analysis within the boundaries of its theoretical assumptions. The derivation of non-deterministic EOB ($\mathbb{E}[\mathcal{B}_z]$) is predicated on idealized conditions: *covariance-stationarity* and *Gaussianity*. However, real-world processes often violate these assumptions, displaying non-stationarity (e.g., evolving trends and volatility) and non-Gaussian traits (e.g., impulsivity and heavy-tailed behavior). *Nevertheless, our theoretical framework provides clear pathways for future*

extension.

One primary extension is to address *non-stationarity* through a *piecewise stationary framework*. This established approach models a non-stationary series as a sequence of distinct, locally stationary segments. Future work could therefore involve a two-stage approach where segment boundaries are first identified using change-point detection algorithms, allowing our EOB theory and SSNR metric to be applied adaptively within each detected stationary regime.

Similarly, while this work adopts GMM as a first step toward handling non-linearity, the *Gaussianity* assumption can be further relaxed. Future work could derive analytical EOB bounds for broader classes of stochastic processes by incorporating more complex, non-Gaussian distributions, such as Lévy skew α -stable or Middleton's class models. This adaptability underscores the potential of our framework as a foundational theory.

G. Characteristic Analysis of DFT, DWT, and Harmonized ℓ_p Norm

G.1. Characteristic of Discrete Fourier Transform

To instantiate the principled debiasing program, we select the Discrete Fourier Transform (DFT) as a principled and effective implementation. For a time series sample $x \in \mathbb{R}^L$, the DFT is a linear projection via a unitary matrix $U \in \mathbb{C}^{K \times L}$ that maps the signal to its complex spectrum $f \in \mathbb{R}^K$

$$f = Ux \quad (89)$$

where the element of U is given by $u_{k,l} = \frac{1}{\sqrt{L}} \exp(-j2\pi kl/L)$.

As a linear, differentiable, and unitary operation, its inverse is simply its conjugate transpose, ensuring a well-defined gradient for optimization.

$$\frac{\partial f}{\partial x} = U^H. \quad (90)$$

The DFT is uniquely suited to our framework for three key advantages that directly align with the goals of proposed debiasing program:

- **Approximate Orthogonality Decomposition:** The DFT decomposes a correlated time series into a set of perfectly uncorrelated frequency components via its trigonometric basis functions. This transformation forces the Structural SNR of the target sequence to its theoretical minimum (*i.e.*, 1), satisfying the independence assumption of the point-wise loss and thus eliminating the optimization bias at its source.
- **Exceptional Computational Effectivity:** The DFT and its inverse are computed with remarkable efficiency using the Fast Fourier Transform (FFT) algorithm, which has a low computational complexity of $\mathcal{O}(L \log L)$. This makes the entire debiasing framework practical even for very long sequences.

In summary, the DFT provides a canonical solution that simultaneously targets both drivers of optimization bias: *it reduces temporal correlation, i.e., SSNR*. While the DFT is a canonical choice, other orthogonal transforms like Wavelet or Chebyshev transforms also represent promising alternatives for future exploration.

G.2. Characteristic of Discrete Wavelet Transform

Discrete Wavelet Transform (DWT) is an alternative effective implementation of principle debiasing program. For a given time series $x \in \mathbb{R}^L$, the DWT performs a multi-resolution analysis via an orthogonal matrix $W \in \mathbb{R}^{L \times L}$ that maps the signal to a set of wavelet coefficients $w \in \mathbb{R}^L$:

$$w = Wx \quad (91)$$

where W is constructed from a chosen mother wavelet (*e.g.*, Haar, Daubechies), and satisfies $W^\top W = I$.

As an orthogonal operation, its inverse is its transpose (W^T), which facilitates seamless backpropagation during training:

$$\frac{\partial w}{\partial x} = W^T \quad (92)$$

The DWT serves as an ideal vehicle for our debiasing framework based on the following structural advantages:

- **Multi-scale Orthogonal Decomposition:** The DWT decomposes a correlated time series into a set of coefficients that are orthogonal across both scale and shift. Unlike the DFT, which uses global trigonometric functions, the DWT uses localized basis functions. This transformation effectively decorrelates the signal, reducing the SSNR of target sequence, thereby mitigating optimization bias.
- **Capture of Non-Stationary Dynamics:** Time series data often exhibit non-stationary behavior where statistical properties change over time. The DWT provides time-frequency localization, allowing the debiasing program to isolate bias not just in frequency bands, but also in specific temporal windows. This makes the framework more robust to structural breaks or transient patterns that a global DFT might smooth over.

- **Linear Computational Complexity:** The DWT and its inverse can be computed with extreme efficiency using the pyramidal algorithm (Mallat's algorithm), which has a computational complexity of $\mathcal{O}(L)$. This is even more efficient than the $\mathcal{O}(L \log L)$ complexity of the FFT, making it the most computationally lean choice for real-time debiasing in long-sequence forecasting.

Summary

In summary, the DWT provides a localized orthogonal solution that targets the drivers of optimization bias with higher granularity than the DFT. By reducing temporal correlation across multiple scales, it optimizes the SSNR while preserving the local structural integrity of the signal.

G.3. Duality of Gradient Flaws in ℓ_p Norms

G.3.1. GRADIENT DOMINANCE IN ℓ_2 NORM

The gradient of ℓ_2 norm is driven by absolute error. For a single predicted component \hat{x}_k , the gradient is:

$$\frac{\partial}{\partial \hat{x}_k} \|x_k - \hat{x}_k\|_2^2 = -2(x_k - \hat{x}_k). \quad (93)$$

To understand the scale dependence, we can express the absolute error as the product of the relative error ($\hat{e}_k = (x_k - \hat{x}_k)/\|x_k\| \in [-1, 1]$) and the true magnitude ($\|x_k\|$). The gradient's magnitude is therefore proportional to $\|x_k\|$. Consequently, high-magnitude components generate overwhelmingly strong gradients, creating a severe *gradient dominance*, rather than the low-magnitude ones is suboptimal.

G.3.2. GRADIENT FATIGUE IN ℓ_1 NORM

Conversely, The gradient of ℓ_1 norm depends only on the *sign* of the error, not its magnitude:

$$\frac{\partial}{\partial \hat{x}_k} \|x_k - \hat{x}_k\|_1 = -\text{sgn}(x_k - \hat{x}_k). \quad (94)$$

The gradient's magnitude is always 1 (or 0). This uniform “push” is too weak for large-magnitude components, which require substantial updates to converge, leading to what we term *gradient fatigue*. Simultaneously, this constant force can be too aggressive for low-magnitude components, causing overshooting and instability.

G.4. Statistical Analysis of Harmonized ℓ_p Norm

G.4.1. POINT ESTIMATION UNBIASEDNESS

First and foremost, a fundamental prerequisite for any valid loss function is *Point Estimation Unbiasedness*. We must ensure that our re-weighting mechanism alters only the optimization dynamics without shifting the theoretical global optimum.

Consider the Harmonized MSE ($\mathcal{L}_{\text{Harm}, \ell_2}$) applied to a specific component k . The loss is defined as the weighted squared Euclidean distance:

$$\mathcal{L}_{\text{Harm}, \ell_2}^k = w_k \|f_k - \hat{f}_k\|_2^2, \quad \text{where} \quad w_k = 1 + \frac{\gamma}{\hat{f}_k + \epsilon} \quad (95)$$

where f_k represents the ground truth and \hat{f}_k denotes the estimation.

Since the weight w_k is strictly positive ($w_k > 0$) and independent of the instantaneous estimation error ($f_k - \hat{f}_k$), calculating the gradient with respect to the estimator \hat{f}_k yields:

$$\frac{\partial \mathcal{L}_{\text{Harm}, \ell_2}^k}{\partial \hat{f}_k} = -2w_k(f_k - \hat{f}_k) \quad (96)$$

Setting the gradient to zero to find the optimal estimator \hat{f}_k^* :

$$-2w_k(f_k - \hat{f}_k) = 0 \implies \hat{f}_k^* = f_k \quad (97)$$

Assuming the ground truth f_k is a realization of the true underlying signal f_k^{true} plus zero-mean noise ξ , *i.e.*, $f_k = f_k^{\text{true}} + \xi$, taking the expectation yields:

$$\mathbb{E}[\hat{f}_k^*] = \mathbb{E}[f_k] = f_k^{\text{true}} \quad (98)$$

For Harmonized MAE ($\mathcal{L}_{\text{Harm}, \ell_1}$), it is also *Point Estimation Unbiasedness* to each element.

$$\mathcal{L}_{\text{Harm}, \ell_1}^k = w_k \|f_k - \hat{f}_k\|_2, \quad \text{where} \quad w_k = 1 + \bar{f}_k \quad (99)$$

$$\frac{\partial \mathcal{L}_{\text{Harm}, \ell_1}^k}{\partial \hat{f}_k} = w_k \text{sgn}(f_k - \hat{f}_k) \quad (100)$$

$$w_k \text{sgn}(f_k - \hat{f}_k) = 0 \implies \hat{f}_k^* = f_k \implies \mathbb{E}[\hat{f}_k^*] = \mathbb{E}[f_k] = f_k^{\text{true}} \quad (101)$$

Conclusion: The Harmonized weighting term w_k scales the gradient magnitude, thereby resolving gradient dominance / fatigue, but it mathematically cancels out at the equilibrium point. Thus, the estimator remains statistically **unbiased**.

G.4.2. ELEMENT BIAS: BALANCING TRAINING STABILITY AND DYNAMICS RECTIFICATION

We generalize Spectral Bias to **Element Bias** to describe the phenomenon where optimization dynamics are dominated by high-magnitude components in any structural orthogonalization (*e.g.*, DFT, DWT, or SVD). While a strictly unbiased loss (*i.e.*, spectral whitening, $\mathcal{L}_{\text{Unbiased}, \ell_2} = \sum_k \|f_k - \hat{f}_k\|_2^2 / \bar{f}_k^2$ and $\mathcal{L}_{\text{Unbiased}, \ell_1} = \sum_k \|f_k - \hat{f}_k\|_2 / \bar{f}_k$) theoretically ensures uniform gradient sensitivity, it is practically pathological due to the uneven Signal-to-Noise Ratio (SNR) distribution. Specifically, strict whitening assigns aggressive weights to noise-dominated low-amplitude components, leading to **training instability** (gradient explosion) and noise overfitting, while simultaneously causing the optimizer to **underfit** the crucial high-amplitude main structures due to their relatively lower gradient contribution.

Our Harmonized Loss resolves this dichotomy by establishing a strategic equilibrium between **Optimization Dynamics Rectification** and **Training Stability** through an adaptive soft-switching mechanism:

- **Stability Anchor (Dominant Regime):** For large-amplitude components, the amplitude ($\nabla_k \mathcal{L}_{\text{Harm}, \ell_2} \propto \bar{f}_k$, $\nabla_k \mathcal{L}_{\text{Harm}, \ell_1} \propto \gamma \bar{f}_k$) harmonized gradient. This deliberately retains the standard norm's focus on fundamental structures, anchoring the optimization trajectory and preventing destabilization by high-frequency noise.
- **Dynamics Rectification (Weak Regime):** For small-amplitude components, the harmonized gradient converges to unity ($\nabla_k \mathcal{L}_{\text{Harm}, \ell_2} \approx \gamma$, $\nabla_k \mathcal{L}_{\text{Harm}, \ell_1} \approx 1$). This acts as an unbiased correction to rectify *gradient fatigue*, ensuring that subtle but informative details receive sufficient gradient flow to be learned effectively.

Conclusion: Element Bias is not blindly eliminated but **adaptively managed**. The Harmonized Loss achieves a Pareto-efficient balance, allowing the model to capture fine-grained details without compromising its grasp on global patterns or succumbing to numerical instability.

G.4.3. INFORMATION-THEORETIC UNBIASEDNESS VIA EOB THEORY

Finally, we connect the proposed Harmonized ℓ_p Norm back to our foundational EOB Theory to demonstrate its information-theoretic consistency.

Recall that EOB is formalized as the Kullback-Leibler (KL) divergence between the true joint distribution $P(\mathcal{X})$ and the factorization $Q(\mathcal{X})$ induced by the point-wise loss function. Standard point-wise losses assume an i.i.d. factorization (Q_{iid}), which leads to a strictly positive EOB when the data possesses temporal structure (*i.e.*, $\text{SSNR} > 1$).

1. Consistency with KL Minimization

Although the Harmonized ℓ_p Norm introduces spectral weights w_k , it remains consistent with the objective of minimizing the KL divergence. Since the weights $w_k(\bar{f}_k)$ are derived from the spectral statistics of the ground truth (acting as a fixed prior) and are independent of the model's estimation parameters θ , the optimization objective $\min \mathcal{L}_{\text{Harm}}$ is equivalent to a *Weighted Maximum Likelihood Estimation*. Crucially, because the weights are strictly positive, the global optimum where $P = Q$ (*i.e.*, $D_{KL}(P||Q) = 0$) remains unchanged. The Harmonized ℓ_p Norm reshapes the *optimization manifold* to accelerate convergence towards this optimum, without shifting the information-theoretic target itself.

2. Asymptotic Unbiasedness at Unit SSNR

A critical test for any debiasing framework is its behavior at the theoretical limit where bias should naturally vanish. According to our quantification of non-deterministic EOB (Theorem 2.6), the lower bound of EOB is monotonically related to the Structural Signal-to-Noise Ratio: $\mathbb{E}[\mathcal{B}_z] \propto \log(SSNR)$.

When condition ($SSNR = 1$): This state corresponds to white noise or a perfectly whitened signal, where spectral energy is uniformly distributed ($\bar{f}_k \approx C, \forall k$) and temporal correlations are absent. The i.i.d. assumption becomes valid, and theoretically, $\mathbb{E}[\mathcal{B}_z] \rightarrow 0$.

Under this condition, the adaptive weights in our Harmonized ℓ_p Norm become uniform:

$$w_k = 1 + \frac{\gamma}{\bar{f}_k} \approx 1 + \frac{\gamma}{C} = \text{const.} \quad (102)$$

Consequently, the loss function degenerates to a scaled version of the standard MSE: $\mathcal{L}_{\text{Harm}} \propto \mathcal{L}_{\text{MSE}}$.

Conclusion: This proves that the Harmonized ℓ_p Norm is **information-theoretically unbiased** in the limit. It introduces no extraneous bias when the data effectively follows an i.i.d. distribution ($SSNR = 1$), while automatically activating its debiasing mechanism only when structural redundancy exists ($SSNR > 1$).

H. Gradient Analysis of Discrete Fourier Transform

In this section, we conduct a rigorous gradient analysis of various DFT application to assess their potential effectiveness.

H.1. Point-wise loss function based on ℓ_2 Norm

We begin by analyzing point-wise loss function based on the ubiquitous ℓ_2 norm.

H.1.1. INDEPENDENT OPTIMIZATION OF REAL AND IMAGINARY COMPONENTS

For a time series sample $x \in \mathbb{R}^L$. DFT can be expressed as a linear projection via a unitary matrix $U \in \mathbb{C}^{K \times L}$:

$$f = Ux \quad (103)$$

where $f \in \mathbb{C}^K$ is the complex spectrum. The elements of the DFT matrix U are given by $u_{k,\tau} = \frac{1}{\sqrt{T}} \exp(-j2\pi k\tau/T)$. Notably, U satisfies $U^H U = \mathbf{I}$, where U^H is the conjugate transpose of U .

We can decompose U into real and imaginary parts, $U = U^r + jU^i$. A common strategy for frequency-domain optimization is to separately penalize the errors in the real and imaginary components of the spectrum:

$$\mathcal{L}_{\text{freq},\ell_2} \triangleq \|\Re(f - \hat{f})\|_2^2 + \|\Im(f - \hat{f})\|_2^2 = \|U^r(x - \hat{x})\|_2^2 + \|U^i(x - \hat{x})\|_2^2 \quad (104)$$

where \hat{x} is the model's predicted and $\hat{f} = U\hat{x}$.

However, a closer examination of this objective reveals a critical flaw. By leveraging the properties of complex numbers and the unitary nature of U , we can simplify $\mathcal{L}_{\text{freq}}$:

$$\begin{aligned} \mathcal{L}_{\text{freq},\ell_2} &= \|U^r(x - \hat{x})\|_2^2 + \|U^i(x - \hat{x})\|_2^2 \\ &= \|U(x - \hat{x})\|_2^2 = \|x - \hat{x}\|_2^2 \\ &\equiv \mathcal{L}_{\text{temp},\ell_2}. \end{aligned} \quad (105)$$

This derivation shows that minimizing the squared ℓ_2 error in the frequency domain is equivalent to minimizing it in the time domain. Consequently, their gradients are identical:

$$\frac{\partial \mathcal{L}_{\text{freq},\ell_2}}{\partial \hat{x}} \equiv \frac{\partial \mathcal{L}_{\text{temp},\ell_2}}{\partial \hat{x}} = -2(x - \hat{x}). \quad (106)$$

This results also can be explained via *Parseval's theorem*.

Theorem H.1. (Ineffectiveness of Unitary Transforms for ℓ_2 Orthogonality) For any unitary transform, minimizing the squared ℓ_2 norm of the transformed error is mathematically equivalent to minimizing the squared ℓ_2 norm of the original error. Therefore, such transforms cannot eliminate optimization bias.

H.1.2. INDEPENDENT OPTIMIZATION OF AMPLITUDE AND PHASE

An alternative approach is to disentangle the objectives by penalizing errors in the amplitude and phase spectra separately. Let the predicted amplitude and phase be \hat{A} and $\hat{\theta}$, respectively,

$$A = |Ux|, \quad \theta = \arg(Ux), \quad (107)$$

$$\mathcal{L}_{A,\ell_2} = \|A - \hat{A}\|_2^2, \quad \mathcal{L}_{\theta,\ell_2} = \|\theta - \hat{\theta}\|_2^2. \quad (108)$$

The gradients of these loss functions with respect to the prediction \hat{x} are:

$$\frac{\partial \mathcal{L}_{A,\ell_2}}{\partial \hat{x}} = -2(U^r)^\top \left((A - \hat{A}) \odot \frac{U^r \hat{x}}{\hat{A}} \right) - 2(U^i)^\top \left((A - \hat{A}) \odot \frac{U^i \hat{x}}{\hat{A}} \right) \quad (109)$$

$$\frac{\partial \mathcal{L}_{\theta,\ell_2}}{\partial \hat{x}} = +2(U^i)^\top \left((\theta - \hat{\theta}) \odot \frac{U^r \hat{x}}{\hat{A}^2} \right) - 2(U^r)^\top \left((\theta - \hat{\theta}) \odot \frac{U^i \hat{x}}{\hat{A}^2} \right) \quad (110)$$

where \odot denotes the Hadamard product.

H.1.3. INDEPENDENT OPTIMIZATION OF ERROR AMPLITUDE AND PHASE

We now consider the amplitude and phase of the error signal itself, $e = x - \hat{x}$:

$$\bar{A} = |Ue|, \quad \bar{\theta} = \arg(Ue) \quad (111)$$

$$\mathcal{L}_{\bar{A}, \ell_2} = \|\bar{A}\|_2^2, \quad \mathcal{L}_{\bar{\theta}, \ell_2} = \|\bar{\theta}\|_2^2. \quad (112)$$

Analyzing the gradient of the error amplitude loss, $\mathcal{L}_{\bar{A}}$, reveals another equivalence:

$$\mathcal{L}_{\bar{A}, \ell_2} = \|U(x - \hat{x})\|_2^2 = \|x - \hat{x}\|_2^2 = \mathcal{L}_{\text{temp}} \quad (113)$$

$$\frac{\partial \mathcal{L}_{\bar{A}, \ell_2}}{\partial \hat{x}} = -2(x - \hat{x}). \quad (114)$$

Once again, simply optimizing the amplitude of the frequency-domain error under the ℓ_2 norm collapses back to the original temporal MSE objective.

However, the gradient for the phase of the error, $\mathcal{L}_{\bar{\theta}}$, provides a unique learning signal:

$$\frac{\partial \mathcal{L}_{\bar{\theta}, \ell_2}}{\partial \hat{x}} = +2(U^r)^\top \left(\bar{\theta} \odot \frac{U^i e}{\bar{A}^2} \right) - 2(U^i)^\top \left(\bar{\theta} \odot \frac{U^r e}{\bar{A}^2} \right). \quad (115)$$

This demonstrates that while penalizing the error amplitude ($\mathcal{L}_{\bar{A}}$) is redundant, penalizing the error phase ($\mathcal{L}_{\bar{\theta}}$) offers a genuinely novel objective.

 H.2. Point-wise loss function based on ℓ_1 Norm

We now investigate whether using the ℓ_1 norm, known for its robustness and different gradient characteristics, can yield more effective disentanglement. The subgradient of the ℓ_1 norm is the sign function, which provides updates of constant magnitude, unlike the ℓ_2 norm's error-proportional updates.

H.2.1. INDEPENDENT OPTIMIZATION OF REAL AND IMAGINARY COMPONENTS

The ℓ_1 analogue to the first ℓ_2 loss is:

$$\mathcal{L}_{\text{freq}, \ell_1} = \|U^r(x - \hat{x})\|_1 + \|U^i(x - \hat{x})\|_1. \quad (116)$$

Its subgradient with respect to \hat{x} is:

$$\frac{\partial \mathcal{L}_{\text{freq}, \ell_1}}{\partial \hat{x}} = -(U^r)^\top \text{sgn}(U^r e) - (U^i)^\top \text{sgn}(U^i e) \quad (117)$$

where $e = x - \hat{x}$. This gradient does not collapse to the temporal ℓ_1 , indicating that it provides a distinct optimization path.

H.2.2. INDEPENDENT OPTIMIZATION OF AMPLITUDE AND PHASE

Applying the ℓ_1 norm to the amplitude and phase of the predictions yields the following objectives:

$$\mathcal{L}_{A, \ell_1} = \|A - \hat{A}\|_1, \quad \mathcal{L}_{\theta, \ell_1} = \|\theta - \hat{\theta}\|_1. \quad (118)$$

The corresponding subgradients are:

$$\frac{\partial \mathcal{L}_{A, \ell_1}}{\partial \hat{x}} = -(U^r)^\top \left(\text{sgn}(A - \hat{A}) \odot \frac{U^r \hat{x}}{\hat{A}} \right) - (U^i)^\top \left(\text{sgn}(A - \hat{A}) \odot \frac{U^i \hat{x}}{\hat{A}} \right) \quad (119)$$

$$\frac{\partial \mathcal{L}_{\theta, \ell_1}}{\partial \hat{x}} = +(U^r)^\top \left(\text{sgn}(\theta - \hat{\theta}) \odot \frac{U^i \hat{x}}{\hat{A}} \right) - (U^i)^\top \left(\text{sgn}(\theta - \hat{\theta}) \odot \frac{U^r \hat{x}}{\hat{A}} \right). \quad (120)$$

H.2.3. INDEPENDENT OPTIMIZATION OF ERROR AMPLITUDE AND PHASE

Finally, we consider the ℓ_1 norm of the error's amplitude and phase:

$$\mathcal{L}_{\bar{A}, \ell_1} = \|\bar{A}\|_1, \quad \mathcal{L}_{\bar{\theta}, \ell_1} = \|\bar{\theta}\|_1. \quad (121)$$

The subgradients are:

$$\begin{aligned} \frac{\partial \mathcal{L}_{\bar{A}, \ell_1}}{\partial \hat{x}} &= -(U^r)^\top \left(\text{sgn}(\bar{A}) \odot \frac{U^r e}{\bar{A}} \right) - (U^i)^\top \left(\text{sgn}(\bar{A}) \odot \frac{U^i e}{\bar{A}} \right) \\ &= -(U^r)^\top \left(\delta(\bar{A}) \odot \frac{U^r e}{\bar{A}} \right) - (U^i)^\top \left(\delta(\bar{A}) \odot \frac{U^i e}{\bar{A}} \right) - \frac{e}{\bar{A}} \\ &\approx -\frac{e}{\bar{A}} \end{aligned} \quad (122)$$

where $\delta(x) = 0$ is the Kronecker Delta function, defined as $\delta(x) = \begin{cases} 1, & \text{if } x = 0 \\ 0, & \text{otherwise} \end{cases}$. The approximate result assumes $\bar{A} > 0$ for all k , the gradient is a vector containing only phase information.

$$\frac{\partial \mathcal{L}_{\bar{\theta}, \ell_1}}{\partial \hat{x}} = +(U^r)^\top \left(\text{sgn}(\bar{\theta}) \odot \frac{U^r e}{\bar{A}^2} \right) - (U^i)^\top \left(\text{sgn}(\bar{\theta}) \odot \frac{U^i e}{\bar{A}^2} \right). \quad (123)$$

Both gradients provide non-trivial and distinct learning signals compared to a simple temporal ℓ_1 loss, confirming that the ℓ_1 norm offers more robust options for objective disentanglement in the frequency domain.

Notably, the structure of these ℓ_1 gradients is analogous to their ℓ_2 counterparts, but the linear error term $2(X - \hat{X})$ or error attribute term $2\bar{X}$ is replaced by the corresponding constant-magnitude $\text{sgn}(X - \hat{X})$ or sign $\text{sgn}(\bar{X})$, respectively, altering the optimization dynamics significantly.

I. Experimental Settings

I.1. Synthetic Dataset Generation Mathematical Mechanism

To empirically validate our theoretical findings, particularly the Paradigm Paradox (Theorem 2.2), we require a process with controllable deterministic and non-deterministic structural components. We therefore construct a synthetic hybrid process x_t by combining a strong, multi-frequency deterministic signal v_t (a sum of sinusoids) with a non-deterministic stochastic process z_t (an $AR(p)$ model):

$$x_t = v_t + z_t = \sum_{i=1}^K A_i \sin\left(\frac{2\pi k_i}{T} t + \varphi_i\right) + \sum_{j=1}^p \phi_j z_{t-j} + \epsilon_t \quad (124)$$

where v_t represents the deterministic component with K harmonics, and z_t is the $AR(p)$ stochastic component driven by innovation noise ϵ_t . A_i , k_i , and φ_i are the amplitude, frequency, and phase of the i -th harmonic, respectively.

Assuming the independence between deterministic $\{v_t\}$ and stochastic $\{z_t\}$ processes, the total variance of the hybrid process $\sigma_x^2 = \text{Var}(x)$ is the sum of the individual variances:

$$\sigma_x^2 = \text{Var}(v) + \text{Var}(z) = \sigma_v^2 + \sigma_z^2 \quad (125)$$

where σ_v^2 and σ_z^2 are the variance of deterministic and stochastic processes, respectively.

We now extend our core metric (Definition 2.4) to this hybrid process. We define the total SSNR of the process, $SSNR_x$, as the ratio of the total process variance σ_x^2 to the variance of the irreducible innovation noise σ_ϵ^2 (*i.e.*, one-step-ahead optimal prediction variance). Thus, $SSNR_x$ is quantified as:

$$SSNR_x = \frac{\sigma_x^2}{\sigma_\epsilon^2} = \frac{\sigma_v^2 + \sigma_z^2}{\sigma_\epsilon^2} = SSNR_v + SSNR_z \quad (126)$$

where $SSNR_v$ and $SSNR_z$ are the SSNRs of deterministic and stochastic components in the hybrid process, respectively.

I.1.1. STATISTICAL PROPERTY OF DETERMINISTIC COMPONENT

We assume the phases φ_i are independent random variables drawn from a uniform distribution $U[0, 2\pi]$. This ensures the deterministic signal v_t has an expected value of zero:

$$\mathbb{E}[v_t] = \mathbb{E}\left[\sum_{i=1}^K A_i \sin\left(\frac{2\pi k_i}{T} t + \varphi_i\right)\right] = \sum_{i=1}^K A_i \mathbb{E}\left[\sin\left(\frac{2\pi k_i}{T} t + \varphi_i\right)\right] = 0. \quad (127)$$

The variance of a single sinusoidal component, when averaged over the random phase φ_i , is $\frac{1}{2}$:

$$\text{Var}\left(\sin\left(\frac{2\pi k_i}{T} t + \varphi_i\right)\right) = \mathbb{E}\left[\sin^2\left(\frac{2\pi k_i}{T} t + \varphi_i\right)\right] = \frac{k_i}{T} \int_0^{\frac{T}{k_i}} \frac{1 - \cos\left(\frac{2\pi k_i}{T} t + \varphi_i\right)}{2} dt = \frac{1}{2}. \quad (128)$$

The K sinusoidal components are mutually orthogonal. Thus, the variance of the deterministic process σ_v^2 is the sum of the variances of sinusoidal components.

$$\sigma_v^2 = \text{Var}\left(\sum_{i=1}^K A_i \sin\left(\frac{2\pi k_i}{T} t + \varphi_i\right)\right) = \sum_{i=1}^K A_i^2 \text{Var}\left(\sin\left(\frac{2\pi k_i}{T} t + \varphi_i\right)\right) = \frac{1}{2} \sum_{i=1}^K A_i^2. \quad (129)$$

In our experiments, we employ an adaptive amplitude adjustment technique to enhance the low-frequency component.

$$A_i = \frac{A\sqrt{K}}{k_i \sqrt{\sum_{j=1}^K 1/k_j^2}} \quad (130)$$

where A denotes the fundamental amplitude and k_i is the randomly selected frequency.

Dataset	Channels	Forecast Horizon	Train / Validation / Test	Frequency	Description
ETTh1	7	96, 192, 336, 720	8545 / 2881 / 2881	Hourly	Oil Temperature
ETTh2	7	96, 192, 336, 720	8545 / 2881 / 2881	Hourly	Oil Temperature
ETTm1	7	96, 192, 336, 720	34465 / 11521 / 11521	15 min	Oil Temperature
ETTm2	7	96, 192, 336, 720	34465 / 11521 / 11521	15 min	Oil Temperature
ECL	321	96, 192, 336, 720	18317 / 2633 / 5261	Hourly	Electricity Consumption
Traffic	862	96, 192, 336, 720	12185 / 1757 / 3509	Hourly	Road Occupancy Rates
Weather	21	96, 192, 336, 720	36792 / 5271 / 10540	10 min	CO_2 Concentration
Exchange	8	96, 192, 336, 720	5120 / 665 / 1422	Daily	Exchange rate
NP	3	96, 192, 336, 720	36500 / 5147 / 10388	Hourly	Electricity Price
PJM	3	96, 192, 336, 720	36500 / 5147 / 10388	Hourly	Electricity Price
BE	3	96, 192, 336, 720	36500 / 5147 / 10388	Hourly	Electricity Price
FR	3	96, 192, 336, 720	36500 / 5147 / 10388	Hourly	Electricity Price
GE	3	96, 192, 336, 720	36500 / 5147 / 10388	Hourly	Electricity Price

Table 3: Benchmark Statistical Description.

Using the equality for the sum of squared amplitudes, $SSNR_v$ is calculated as follows:

$$\sum_{i=1}^K A_i^2 = \sum_{i=1}^K \frac{KA^2/k_i^2}{\sum_{j=1}^K 1/k_j^2} = KA^2, \quad (131)$$

$$SSNR_v = \frac{KA^2}{2\sigma_\epsilon^2}. \quad (132)$$

I.1.2. STATISTICAL PROPERTY OF STOCHASTIC COMPONENT

We set a autoregressive process with $p = 1$ as stochastic component. For any covariance-stationary process, the stochastic variance σ_z^2 is control by autoregressive coefficient (ϕ_1) and variance of innovation noise (σ_ϵ^2) regardless of the distribution of innovation noise:

$$\sigma_z^2 = \frac{\sigma_\epsilon^2}{1 - \phi_1^2}. \quad (133)$$

We control the autoregressive coefficient (ϕ_1) to adjust $SSNR_z$ with arbitrarily distributed noise,

$$SSNR_z = \frac{\sigma_z^2}{\sigma_\epsilon^2} = \frac{1}{1 - \phi_i^2} \Rightarrow \phi_1 = \sqrt{\frac{SSNR_z - 1}{SSNR_z}}. \quad (134)$$

Consequently, we have the precise formula of $SSNR_x$:

$$SSNR_x = SSNR_v + SSNR_z = \frac{KA^2}{2\sigma_\epsilon^2} + \frac{1}{1 - \phi^2}. \quad (135)$$

I.2. Real-world Benchmark Description

Our empirical validation relies on a diverse suite of real-world benchmarks, detailed in Table 3. These datasets were selected to represent a wide range of domains, temporal resolutions, and challenging structural characteristics:

- **ETT** (Electricity Transformer Temperature) (Zhou et al., 2021): The ETT dataset includes two hourly-level datasets (ETTh1 and ETTh2) and two 15-minute-level datasets (ETTm1 and ETTm2). Each dataset includes 7 oil and load features of electricity transformers from July 2016 to July 2018.
- **ECL** (Electricity Consumption Load) (Wu et al., 2021): The ECL dataset records the hourly electricity consumption of 321 distinct clients from 2012 to 2014.
- **Traffic** (Wu et al., 2021): The Traffic dataset contains hourly road occupancy rates obtained from sensors located on San Francisco freeways from 2015 to 2016.
- **Weather** (Wu et al., 2021): The Weather dataset contains 21 indicators of weather(*e.g.*, air temperature and humidity), which are collected in Germany. The data is recorded at a high frequency of every 10 minutes.
- **Exchange** (Lai et al., 2018): The Exchange dataset records the daily exchange rates of eight different countries relative to the US dollar, ranging from 1990 to 2016.
- **PJM** (Lago et al., 2021): The PJM dataset represents the Pennsylvania-New Jersey-Maryland market, which contains the zonal electricity price within the Commonwealth Edison (COMED) zone, and the corresponding System load and COMED load forecast from 2013-01-01 to 2018-12-24.
- **BE** (Lago et al., 2021): The BE dataset represents the Belgium electricity market, recording the hourly electricity price, the load forecast in Belgium and the generation forecast in France from 2011-01-09 to 2016-12-31.
- **FR** (Lago et al., 2021): The FR dataset represents the electricity market in France, recording the hourly prices, and corresponding load and generation forecast from 2012-01-09 to 2017-12-31.

I.3. Backbone Description

Transformer-based methods:

- **iTransformer** (Liu et al., 2024) introduces an “inverted” transformer architecture that swaps the roles of queries, keys, and values to simplify and accelerate time series modeling.
- **PatchTST** (Nie et al., 2023) treats a time series as a sequence of fixed-length patches and applies Transformer-based patch-wise modeling to capture long-range dependencies.
- **Pyraformer** (Liu et al., 2022) proposes the pyramidal attention module (PAM) to capture multi-scale temporal dependencies with $O(N)$ linear complexity, effectively handling long sequences.
- **FEDformer** (Zhou et al., 2022) leverages frequency-enhanced decomposition within a transformer framework to efficiently model and forecast long-term periodic patterns.
- **Autoformer** (Wu et al., 2021) replaces the traditional self-attention mechanism with the Auto-Correlation mechanism to discover period-based dependencies and incorporates a basic inner block of deep models.
- **Transformer** (Vaswani et al., 2017) utilizes a self-attention mechanism to capture global dependencies across the entire sequence, serving as a fundamental baseline for sequence modeling.

MLP-based methods:

- **TimeMixer** (Wang et al., 2024) introduces Past-Decomposable-Mixing (PDM) and Future-Multipredictor-Mixing (FMM) blocks, effectively handling multiscale series.
- **TSMixer** (Ekambaram et al., 2023) operates in both the time and feature dimensions to extract information, efficiently utilizing cross-variate and auxiliary information
- **DLinear** (Zeng et al., 2023) decomposes the series into trend and seasonal components, fits each with a simple linear model, and then recombines them for forecasting.

Innovation Noise	Continuity	Symmetry	Support Set	Tail	Peak Degree	Parameters
Binomial	✗	Approx. Sym.	$\{0, 1, \dots, n\}$	None	< 3	$n = 1, p = 0.5$
Geometric	✗	Right-leaning	$\{1, 2, \dots\}$	Heavy	—	$p = 2(\sqrt{2} - 1)$
Gaussian	✓	✓	$(-\infty, \infty)$	Middle	3	$\mu = 0, \sigma = 0.5$
Poisson	✗	Approx. Sym.	$\{0, 1, \dots\}$	Middle	≈ 3	$\lambda = 0.5$
Student's t	✓	✓	$(-\infty, \infty)$	Heavy	> 3	$\nu = 5, \alpha = \sqrt{15}/10$
Cont. Uniform	✓	✓	$[a, b]$	None	1.8	$b = -a = \sqrt{3}/2$

Table 4: Innovation Noise Distribution Parameter Settings. We set the variance of innovation noise to be $\sigma_\epsilon^2 = 0.25$.

- **FreTS** (Yi et al., 2023a) utilizes MLPs in the frequency domain, capture global dependencies with lower computational complexity.

CNN-based methods:

- **TimesNet** (Wu et al., 2023) constructs a 2D temporal-variation representation and applies joint time–frequency convolutions to capture general patterns in time series data.
- **MICN** (Wang et al., 2023) designs a multi-scale isometric convolution network that combines down-sampled convolution with isometric convolution to capture local features and global correlations simultaneously.

Others:

- **FreDF** (Wang et al., 2025b) proposes learning to forecast in the frequency domain, reducing estimation bias caused by label autocorrelation.

I.4. Implementation Details

I.4.1. FOR EOB THEORY VERIFICATION EXPERIMENT

We set $A^2 = [0, 1, 2, 3, 4, 5, 6, 7, 8, 9]$ to ensure comprehensive coverage. Correspondingly, the total SSNR, $SSNR_x$, ranges from 32 to 320 with an interval of 32. Specifically, when $SSNR_x = 32$, series reduces to purely stochastic $AR(1)$ process.

For each $SSNR_x$ value, we generate 100 time series of length 5000, with a The training/test split ratio set to 0.7/0.3. We randomly select one time series for experimental validation and sample sub-series with a stride of 1 to construct the dataset.

The history windows size is fixed at $H = 128$, and the forecast horizon is set to multiples of the history windows size, *i.e.*, $h = 128 \times n$ for $n = 1, 2, \dots, 10$.

To ensure statistical reliability, each result is the average of 25 independent experiments with different random seeds.

We adopt the *Adam Optimizer* for model parameter optimization and the *early stop technique* to mitigate overfitting.

To effectively simulate actual data distributions and comprehensively validate our EOB Theory, we conducted grid experiments across 5 kinds of foundational deep learning architectures and 6 categories of innovation noise distributions.

Foundational deep learning architectures: CNN, LSTM, MLP, ModernTCN, and Transformer.

Innovation noise is modeled by a distribution with variance σ_ϵ^2 , which can be categorized into discrete vs. continuous, symmetrical vs. asymmetrical, and heavy-tailed vs. light-tailed types. The characteristics and parameter settings of each distribution are summarized in Table 4.

- **Binomial Distribution** is the discrete probability distribution of the number of successes in a sequence of n independent experiments, each asking a yes–no question.

Probability Mass Function:

$$P(X = k) = \binom{n}{k} p^k (1 - p)^{n - k}$$

Statistical Properties:

$$\mathbb{E}[X] = \frac{1}{p}; \quad \text{Var}(X) = np(1-p)$$

Configure Parameters:

$$n = 1; \quad p = \frac{1 \pm \sqrt{1 - 4\sigma_\epsilon^2}}{2}$$

- **Geometric Distribution** gives the probability that the first occurrence of success requires k independent trials, each with success probability p .

Probability Mass Function:

$$F_X(k) = P(X \leq k) = 1 - (1-p)^k, \quad k = 1, 2, \dots$$

Statistical Properties:

$$\mathbb{E}[X] = \frac{1}{p}; \quad \text{Var}(X) = \frac{1-p}{p^2}$$

Configure Parameters:

$$p = \frac{-1 + \sqrt{1 + 4\sigma_\epsilon^2}}{2\sigma_\epsilon^2}$$

- **Gaussian Distribution** is important in statistics and are often used in the natural and social sciences to represent real-valued random variables whose distributions are not known.

Probability Mass Function:

$$P(X) = \frac{1}{\sqrt{2\pi\sigma^2}} \exp\left(-\frac{(x-\mu)^2}{2\sigma^2}\right)$$

Configure Parameters:

$$\mu = 0; \quad \sigma = \sigma_\epsilon$$

- **Poisson Distribution** is a discrete probability distribution that expresses the probability of a given number of events occurring in a fixed interval of time if these events occur with a known constant mean rate and independently of the time since the last event.

Probability Mass Function:

$$P(X = k) = \begin{cases} \frac{\lambda^k e^{-\lambda}}{k!}, & k = 0, 1, 2, \dots, \\ 0, & \text{otherwise,} \end{cases}$$

Statistical Properties:

$$\mathbb{E}[X] = \lambda; \quad \text{Var}(X) = \lambda$$

Configure Parameters:

$$\lambda = \sigma_\epsilon$$

- **Student's t Distribution** is a continuous probability distribution that generalizes the standard normal distribution, but has heavier tails, and the amount of probability mass in the tails is controlled by the parameter ν .

Probability Mass Function:

$$P(X; \nu) = \frac{\Gamma(\frac{\nu+1}{2})}{\sqrt{\pi\nu}\Gamma(\frac{\nu}{2})} \left(1 + \frac{X^2}{\nu}\right)^{-(\nu+1)/2}$$

where $\Gamma(\cdot)$ is the gamma function.

Statistical Properties:

$$\mathbb{E}[X] = \begin{cases} 0, & \nu > 1 \\ \text{Does not exist,} & \nu \leq 1 \end{cases}, \quad \text{Var}(X) = \begin{cases} \frac{\nu}{\nu-2}, & \nu > 2 \\ \text{Does not exist,} & \nu \leq 2 \end{cases}$$

Configure Parameters:

$$\nu = 5, \quad \alpha = \sigma_\epsilon \sqrt{\frac{\nu-2}{\nu}}, \quad F'(X, \nu) = \alpha F(X, \nu)$$

- **Continuous Uniform Distribution** describes an experiment where there is an arbitrary outcome that lies between certain bounds. The bounds are defined by the parameters, a and b , which are the minimum and maximum values.

Probability Mass Function:

$$P(X) = \begin{cases} \frac{1}{b-a}, & \text{if } a \leq x \leq b \\ 0, & \text{otherwise} \end{cases}$$

Statistical Properties:

$$\mathbb{E}[X] = \frac{b-a}{2}, \quad \text{Var}(X) = \frac{(b-a)^2}{12}$$

Configure Parameters:

$$b = -a = \sqrt{3}\sigma_\epsilon$$

I.4.2. FOR LONG-TERM FORECASTING TASKS

The baseline models are reproduced using the scripts provided by (Wu et al., 2023) which employs Adam optimizer to minimize the target loss. Datasets are split chronologically into training, validation, and test sets with the ratio of 6:2:2. Following the protocol outlined in the comprehensive benchmark (Qiu et al., 2024), the dropping-last trick is disabled during the test phase.

J. Experimental Results

J.1. Empirical Verification of EOB Theory

To validate the generality of our EBO Theory, we experiment with *six distinct innovation noise distributions*, encompassing Binomial, Geometric, Gaussian, Poisson, Student's t , and Continuous Uniform, which span discrete / continuous, symmetrical / asymmetrical, and heavy-tailed / light-tailed properties. We test these across *five fundamental architectures*: CNN, LSTM, MLP, ModernTCN, and Transformer. The experimental results for each architecture-innovation combination are presented in Figures 4 - 8, displaying (a) actual MSE, (b) relative MSE, (c) optimal relative, and (d) inefficiency ratio surfaces.

Regardless of the architecture-innovation combination, performance and evolutionary pattern of corresponding surface are consistent, validating the universality of our EOB Theory which holds irrespective of specific innovation distribution or model architecture employed.

Detailed error dynamics analysis and explanation of phenomenon are provided in Section 6.2 of main text.

J.2. Long-term Forecasting

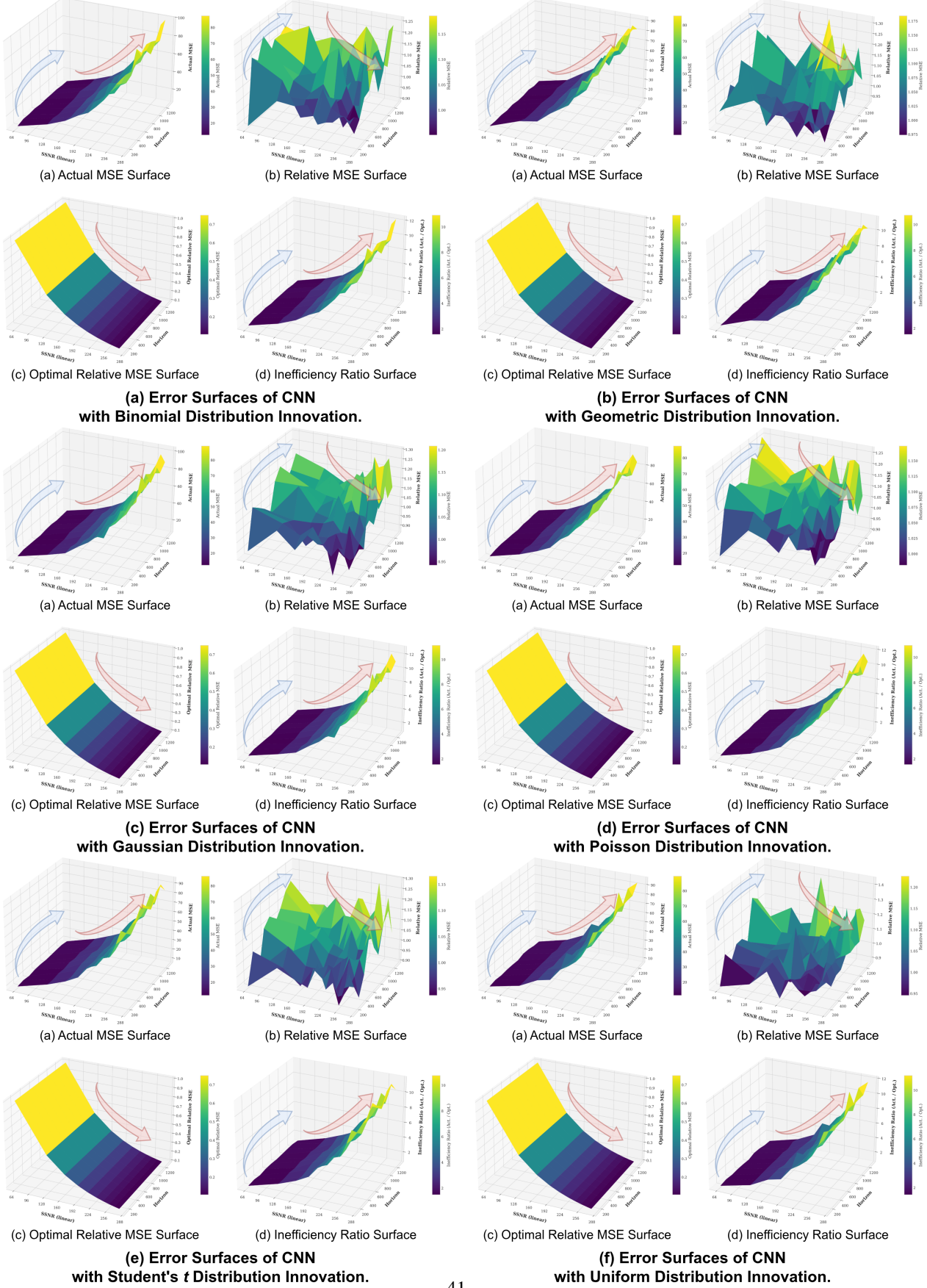


Figure 4: Empirical verification of EOB Theory via CNN model. The blue and red arrows indicates the surface variation trend along horizon h and the total SSNR $SSNR_x$, respectively.

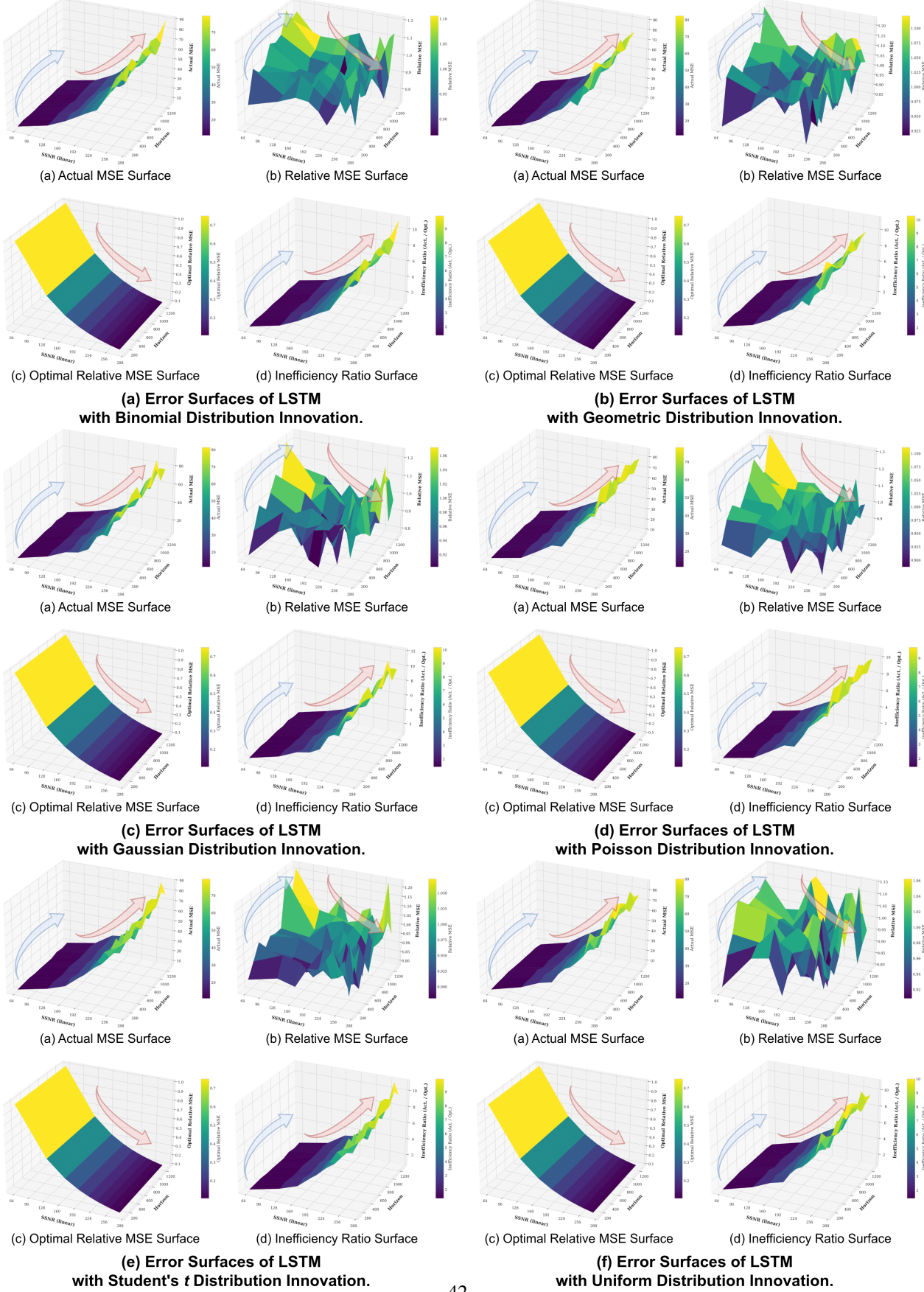


Figure 5: Empirical verification of EOB Theory via LSTM model. The blue and red arrows indicates the surface variation trend along horizon h and the total SSNR $SSNR_x$, respectively.

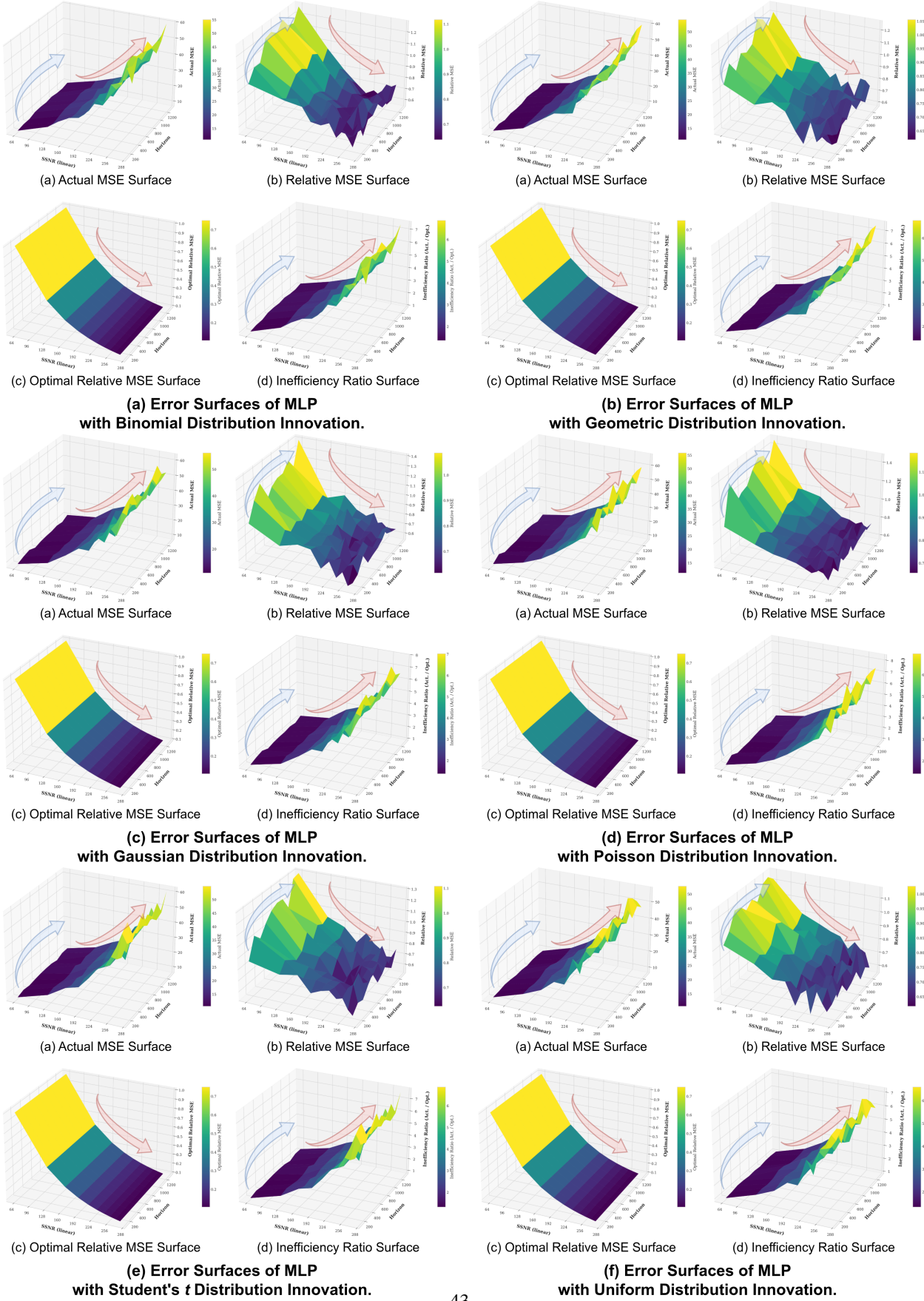


Figure 6: Empirical verification of EOB Theory via MLP model. The blue and red arrows indicates the surface variation trend along horizon h and the total SSNR $SSNR_x$, respectively.

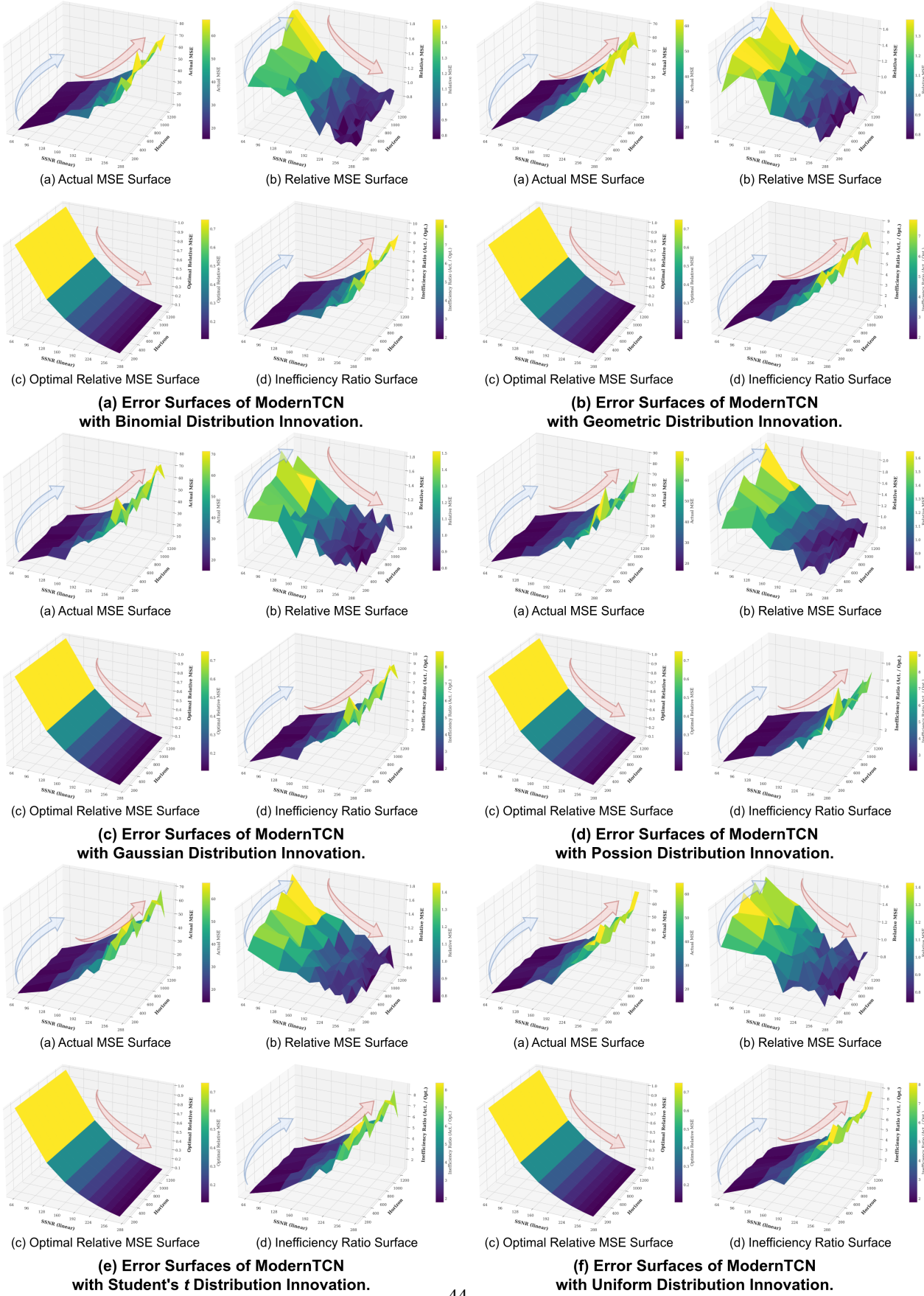


Figure 7: Empirical verification of EOB Theory via ModernTCN model. The blue and red arrows indicates the surface variation trend along horizon h and the total SSNR $SSNR_x$, respectively.

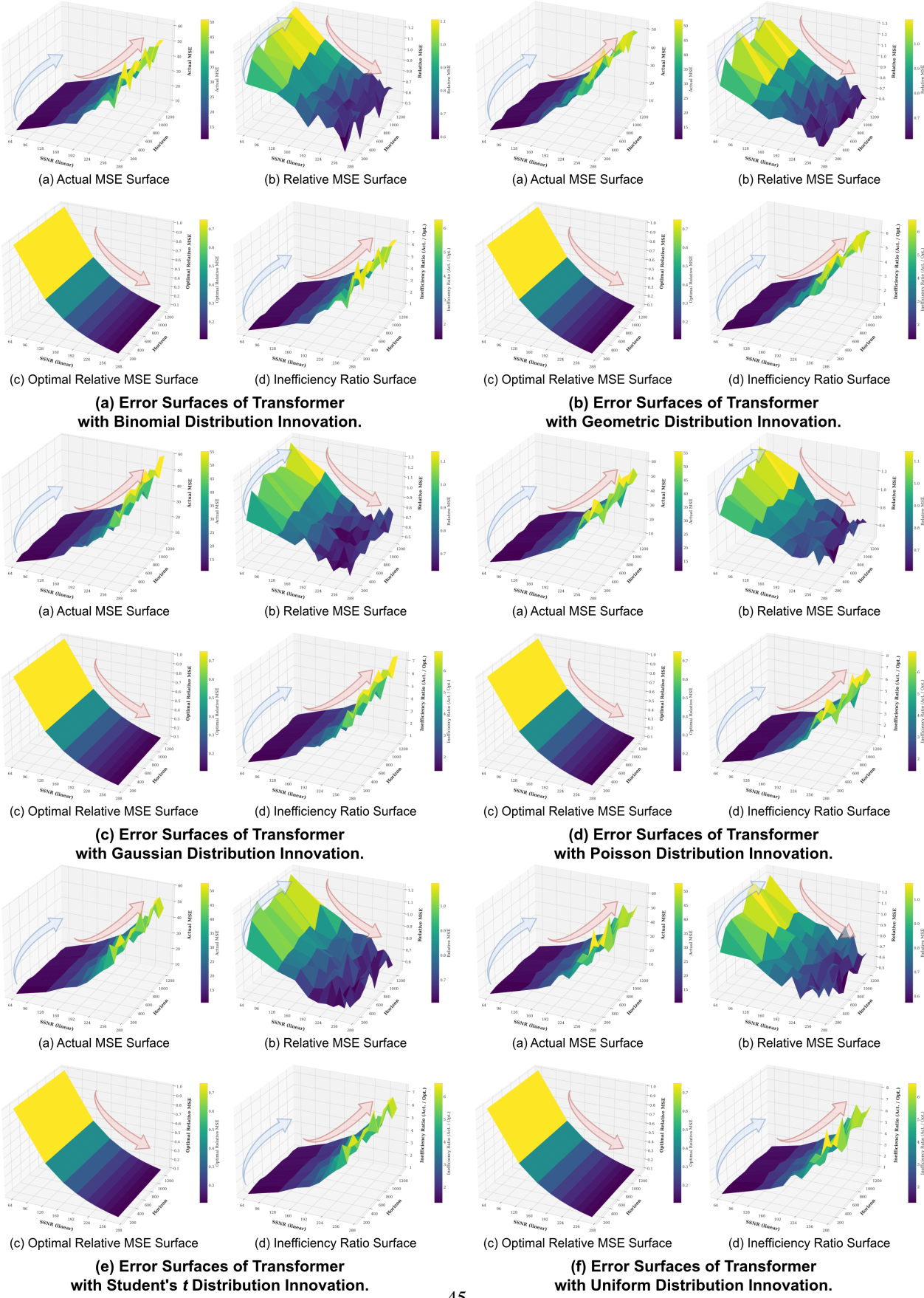


Figure 8: Empirical verification of EOB Theory via Transformer model. The blue and red arrows indicates the surface variation trend along horizon h and the total SSNR $SSNR_x$, respectively.

Models	$\mathcal{L}_{\text{Ham}, \ell_p}$		FreDF (2025)	TimeMixer (2024)	iTransformer (2024)	PatchTST (2023)	TimesNet (2023)	TSMixer (2023)	DLinear (2023)	FreTS (2023)	MICN (2023)	Pyraformer (2022)	FEDformer (2022)	Autoformer (2021)	Transformer (2017)	
Metrics	MSE	MAE	MSE	MAE	MSE	MAE	MSE	MAE	MSE	MAE	MSE	MAE	MSE	MAE	MSE	MAE
ETTh1	96 0.379 0.389 0.378 0.396 0.382 0.399 0.393 0.408 0.382 0.400 0.412 0.428 0.495 0.504 0.396 0.411	0.398 0.410 0.421 0.435 0.380 0.420 0.466 0.476 0.380 0.420 0.446 0.464 0.921 0.762														
	192 0.427 0.419 0.428 0.423 0.437 0.430 0.447 0.440 0.430 0.433 0.457 0.453 0.588 0.562 0.446 0.442	0.455 0.447 0.489 0.479 0.830 0.702 0.431 0.450 0.503 0.486 0.106 0.825														
	336 0.464 0.438 0.469 0.444 0.485 0.452 0.489 0.463 0.474 0.460 0.506 0.479 0.678 0.617 0.488 0.466	0.504 0.475 0.580 0.543 1.003 0.790 0.467 0.469 1.136 0.868														
	720 0.460 0.460 0.505 0.493 0.518 0.488 0.514 0.499 0.529 0.508 0.523 0.498 0.760 0.678 0.512 0.510	0.564 0.539 0.734 0.640 1.009 0.804 0.500 0.534 0.521 0.602 0.830														
Avg 0.433 0.426 0.445 0.439 0.455 0.443 0.461 0.453 0.454 0.450 0.475 0.464 0.630 0.590 0.461 0.457	0.480 0.468 0.556 0.524 0.893 0.735 0.446 0.460 0.506 0.492 1.045 0.821															
ETTh2	96 0.286 0.333 0.288 0.337 0.295 0.345 0.303 0.353 0.297 0.349 0.336 0.373 1.144 0.871 0.360 0.405	0.411 0.396 0.360 0.405 1.189 0.862 0.340 0.384 0.362 0.400 1.046														
	192 0.367 0.384 0.376 0.393 0.377 0.397 0.380 0.401 0.374 0.398 0.418 0.422 1.627 1.054 0.488 0.476	0.485 0.476 0.487 0.478 3.182 1.478 0.422 0.434 0.438 0.444 4.162 1.719														
	336 0.412 0.420 0.419 0.427 0.436 0.436 0.431 0.439 0.423 0.435 0.458 0.455 1.753 1.099 0.608 0.550	0.571 0.532 0.598 0.542 3.887 1.739 0.457 0.468 0.462 0.469 3.540 1.574														
	720 0.420 0.437 0.424 0.442 0.445 0.453 0.436 0.452 0.437 0.455 0.468 0.470 1.929 1.166 0.853 0.667	0.777 0.638 0.834 0.659 3.720 1.687 0.487 0.490 0.473 0.485 3.266 1.531														
Avg 0.371 0.393 0.377 0.400 0.388 0.408 0.390 0.412 0.383 0.409 0.420 0.430 1.613 1.048 0.577 0.528	0.542 0.510 0.570 0.521 2.994 1.441 0.427 0.444 0.434 0.450 3.153 1.468															
ETTm1	96 0.326 0.353 0.329 0.362 0.322 0.360 0.349 0.379 0.327 0.367 0.334 0.375 0.469 0.467 0.355 0.379	0.353 0.386 0.319 0.370 0.598 0.525 0.381 0.423 0.532 0.490 0.502 0.508														
	192 0.373 0.377 0.377 0.388 0.365 0.385 0.388 0.397 0.371 0.391 0.389 0.403 0.482 0.484 0.389 0.396	0.394 0.407 0.364 0.402 0.620 0.554 0.417 0.438 0.608 0.522 0.736 0.639														
	336 0.407 0.398 0.411 0.409 0.395 0.407 0.424 0.420 0.399 0.408 0.417 0.423 0.538 0.523 0.419 0.418	0.431 0.433 0.409 0.437 0.716 0.625 0.465 0.464 0.635 0.534 1.051 0.798														
	720 0.465 0.432 0.482 0.448 0.458 0.444 0.494 0.459 0.460 0.446 0.490 0.461 0.633 0.581 0.477 0.454	0.496 0.473 0.512 0.503 0.898 0.720 0.506 0.487 0.628 0.537 1.114 0.813														
Avg 0.393 0.390 0.400 0.402 0.385 0.399 0.414 0.414 0.390 0.403 0.407 0.416 0.531 0.514 0.410 0.412	0.419 0.424 0.401 0.428 0.708 0.606 0.442 0.453 0.601 0.521 0.855 0.689															
ETTm2	96 0.175 0.253 0.177 0.256 0.175 0.258 0.184 0.270 0.183 0.266 0.189 0.269 0.298 0.411 0.200 0.301	0.197 0.294 0.190 0.287 0.411 0.479 0.200 0.285 0.221 0.304 0.366 0.461														
	192 0.240 0.296 0.241 0.298 0.240 0.301 0.252 0.313 0.248 0.309 0.254 0.311 0.487 0.545 0.289 0.367	0.277 0.353 0.281 0.354 0.625 0.324 0.275 0.333 0.330 0.320 0.866 0.713														
	336 0.301 0.336 0.302 0.337 0.299 0.341 0.316 0.353 0.311 0.349 0.320 0.349 0.851 0.742 0.387 0.373	0.418 0.419 0.373 0.419 1.116 0.807 0.327 0.364 0.331 0.368 1.231 0.846														
	720 0.401 0.394 0.401 0.395 0.397 0.398 0.412 0.406 0.412 0.407 0.417 0.406 2.106 1.230 0.547 0.521	0.535 0.510 0.550 0.514 3.716 1.465 0.427 0.422 0.427 0.421 3.133 1.348														
Avg 0.279 0.320 0.280 0.321 0.278 0.325 0.291 0.335 0.288 0.333 0.295 0.334 0.935 0.732 0.356 0.405	0.345 0.394 0.350 0.394 1.494 0.851 0.305 0.348 0.313 0.357 1.399 0.842															
ECL	96 0.178 0.268 0.144 0.233 0.216 0.318 0.148 0.240 0.180 0.272 0.171 0.276 0.216 0.318 0.252 0.347	0.191 0.279 0.198 0.308 0.294 0.384 0.219 0.329 0.210 0.324 0.276 0.374														
	192 0.187 0.275 0.159 0.249 0.225 0.333 0.165 0.256 0.192 0.282 0.190 0.293 0.225 0.333 0.235 0.350	0.195 0.283 0.211 0.319 0.324 0.409 0.208 0.321 0.235 0.340 0.302 0.396														
	336 0.200 0.291 0.172 0.264 0.247 0.355 0.179 0.272 0.208 0.298 0.206 0.309 0.247 0.355 0.264 0.362	0.208 0.298 0.224 0.333 0.336 0.419 0.227 0.340 0.255 0.357 0.320 0.406														
	720 0.247 0.321 0.206 0.294 0.286 0.383 0.213 0.301 0.250 0.330 0.238 0.331 0.286 0.383 0.247 0.354	0.232 0.343 0.333 0.412 0.273 0.375 0.314 0.403 0.351 0.408 0.331 0.408														
Avg 0.203 0.289 0.171 0.260 0.243 0.347 0.176 0.267 0.208 0.296 0.201 0.302 0.243 0.347 0.266 0.362	0.210 0.299 0.216 0.326 0.322 0.406 0.232 0.341 0.253 0.356 0.307 0.396															
Traffic	96 0.468 0.291 0.391 0.265 0.476 0.296 0.393 0.269 0.471 0.307 0.593 0.316 0.538 0.366 0.780 0.476	0.532 0.342 0.516 0.310 0.693 0.398 0.594 0.376 0.625 0.391 0.663 0.366														
	192 0.476 0.291 0.410 0.274 0.497 0.308 0.413 0.277 0.477 0.309 0.616 0.328 0.548 0.377 0.647 0.407	0.532 0.339 0.536 0.317 0.684 0.390 0.611 0.381 0.648 0.409 0.700 0.369														
	336 0.488 0.307 0.424 0.280 0.506 0.314 0.424 0.283 0.492 0.314 0.631 0.337 0.566 0.385 0.653 0.410	0.550 0.345 0.547 0.321 0.691 0.391 0.627 0.394 0.629 0.392 0.676 0.370														
	720 0.525 0.325 0.460 0.298 0.534 0.321 0.458 0.300 0.526 0.332 0.661 0.351 0.694 0.429 0.600 0.367 0.572	0.331 0.231 0.722 0.405 0.648 0.399 0.664 0.410 0.692 0.376 0.707 0.376														
Avg 0.489 0.296 0.421 0.279 0.503 0.310 0.422 0.282 0.491 0.316 0.625 0.333 0.566 0.385 0.694 0.430	0.554 0.320 0.697 0.396 0.620 0.387 0.641 0.401 0.675 0.370															
Weather	96 0.174 0.209 0.172 0.211 0.163 0.210 0.176 0.217 0.178 0.219 0.172 0.221 0.179 0.250 0.196 0.257	0.184 0.239 0.192 0.250 0.189 0.276 0.220 0.299 0.287 0.349 0.354 0.405														
	192 0.222 0.251 0.224 0.256 0.208 0.251 0.225 0.258 0.224 0.259 0.231 0.270 0.217 0.285 0.237 0.296	0.237 0.276 0.224 0.324 0.243 0.324 0.288 0.351 0.320 0.372 0.555 0.522														
	336 0.277 0.291 0.280 0.297 0.264 0.292 0.289 0.298 0.280 0.299 0.284 0.305 0.261 0.319 0.283 0.331	0.333 0.364 0.304 0.364 0.300 0.364 0.347 0.405 0.320 0.373 0.691 0.590														
	720 0.353 0.340 0.360 0.351 0.345 0.354 0.345 0.350 0.356 0.348 0.360 0.351 0.317 0.359 0.347 0.361	0.361 0.394 0.321 0.422 0.342 0.422 0.377 0.437 0.357 0.439 0.692 0.513														
Avg 0.257 0.273 0.259 0.279 0.245 0.275 0.260 0.281 0.262 0.288 0.244 0.304 0.266 0.317 0.255 0.299	0.267 0.299 0.261 0.316 0.231 0.316 0.286 0.348 0.272 0.316 0.697 0.557															
Exchange	96 0.084 0.201 0.112 0.241 0.085 0.202 0.090 0.212 0.089 0.207 0.118 0.245 0.591 0.574 0.116 0.258	0.091 0.221 0.110 0.251 0.090 0.221 0.179 0.250 0.157 0.286 0.287 0.629														
	192 0.183 0.304 0.207 0.328 0.180 0.301 0.307 0.307 0.217 0.337 0.738 0.639 0.206 0.347	0.347 0.322 0.209 0.356 0.219 0.347 0.321 0.356 0.296 0.396 1.136 0.825														
	336 0.343 0.424 0.380 0.450 0.340 0.422 0.337 0.421 0.352 0.431 0.404 0.465 0.966 0.757 0.329 0.447	0.457 0.450 0.559 0.609 0.387 0.450 0.375 0.445 0.464 0.500 1.323 0.975														
	720 0.877 0.709 0.967 0.749 0.871 0.702 0.857 0.704 0.885 0.708 1.020 0.774 1.451 0.927 0.529 0.572	0.862 0.700 1.227 0.906 1.909 1.126 1.161 0.829 1.160 0.837 1.553 1.007														
Avg 0.372 0.409 0.416 0.442 0.369 0.407 0.367 0.411 0.378 0.413 0.440 0.455 0.937 0.724 0.295 0.406	0.377 0.426 0.526 0.531 1.328 0.930 0.509 0.496 0.519 0.506 1.167 0.859															
BE	96 0.235 0.258 0.244 0.246 0.290 0.309 0.269 0.284 0.248 0.273 0.259 0.281 0.364 0.383 0.326 0.348	0.293 0.313 0.257 0.302 0.269 0.301 0.301 0.327 0.248 0.317 0.277 0.270														
	192 0.274 0.288 0.294 0.299 0.295 0.303 0.277 0.291 0.271 0.297 0.294 0.301 0.364 0.387 0.342 0.364	0.313 0.324 0.260 0.292 0.279 0.308 0.260 0.308 0.247 0.311 0.328 0.346														
	336 0.315 0.326 0.355 0.335 0.346 0.338 0.336 0.321 0.333 0.326 0.336 0.424 0.379 0.356 0.360 0.306	0.334 0.317 0.268 0.294 0.309 0.321 0.306 0.317 0.247 0.311 0.328 0.340														
	720 0.392 0.386 0.449 0.410 0.477															